ResearchGate

See discussions, stats, and author profiles for this publication at: https://www.researchgate.net/publication/328854439

# Science and technology of ammonia combustion

**Article** *in* Proceedings of the Combustion Institute · November 2018

DOI: 10.1016/j.proci.2018.09.029

CITATIONS
246

READS
7,726

**4 authors:**

Hideaki Kobayashi
Kanagawa University
**170** PUBLICATIONS **3,403** CITATIONS
SEE PROFILE

Akihiro Hayakawa
Tohoku University
**100** PUBLICATIONS **1,678** CITATIONS
SEE PROFILE

Kapuruge Don Kunkuma Amila Somarathne
Tohoku University
**17** PUBLICATIONS **724** CITATIONS
SEE PROFILE

Ekenechukwu C Okafor
National Institute of Advanced Industrial Science and Technology
**37** PUBLICATIONS **820** CITATIONS
SEE PROFILE

**Some of the authors of this publication are also working on these related projects:**



Liquid Ammonia Spray Combustion in Gas Turbines View project



Elucidation of fundamental combustion characteristics of ammonia/hydrogen/methane blended fuels to develop and optimize the design of low carbon gas turbines for power plants View project

All content following this page was uploaded by Ekenechukwu C Okafor on 01 February 2019.

The user has requested enhancement of the downloaded file.

Available online at www.sciencedirect.com

ScienceDirect

Proceedings of the Combustion Institute 37 (2019) 109–133

Proceedings of the Combustion Institute

www.elsevier.com/locate/proci

# Science and technology of ammonia combustion

Hideaki Kobayashi*, Akihiro Hayakawa, K.D. Kunkuma A. Somarathne, Ekenechukwu C. Okafor

*Institute of Fluid Science, Tohoku University, Sendai, Miyagi 980-8577, Japan*

Received 1 December 2017; accepted 13 September 2018
Available online 9 November 2018

**Abstract**

This paper focuses on the potential use of ammonia as a carbon-free fuel, and covers recent advances in the development of ammonia combustion technology and its underlying chemistry. Fulfilling the COP21 Paris Agreement requires the de-carbonization of energy generation, through utilization of carbon-neutral and overall carbon-free fuels produced from renewable sources. Hydrogen is one of such fuels, which is a potential energy carrier for reducing greenhouse-gas emissions. However, its shipment for long distances and storage for long times present challenges. Ammonia on the other hand, comprises 17.8% of hydrogen by mass and can be produced from renewable hydrogen and nitrogen separated from air. Furthermore, thermal properties of ammonia are similar to those of propane in terms of boiling temperature and condensation pressure, making it attractive as a hydrogen and energy carrier. Ammonia has been produced and utilized for the past 100 years as a fertilizer, chemical raw material, and refrigerant. Ammonia can be used as a fuel but there are several challenges in ammonia combustion, such as low flammability, high NOx emission, and low radiation intensity. Overcoming these challenges requires further research into ammonia flame dynamics and chemistry. This paper discusses recent successful applications of ammonia fuel, in gas turbines, co-fired with pulverize coal, and in industrial furnaces. These applications have been implemented under the Japanese 'Cross-ministerial Strategic Innovation Promotion Program (SIP): Energy Carriers'. In addition, fundamental aspects of ammonia combustion are discussed including characteristics of laminar premixed flames, counterflow twin-flames, and turbulent premixed flames stabilized by a nozzle burner at high pressure. Furthermore, this paper discusses details of the chemistry of ammonia combustion related to NOx production, processes for reducing NOx, and validation of several ammonia oxidation kinetics models. Finally, LES results for a gas-turbine-like swirl-burner are presented, for the purpose of developing low-NOx single-fuelled ammonia gas turbine combustors.
© 2019 The Authors. Published by Elsevier Inc. on behalf of The Combustion Institute.
This is an open access article under the CC BY license. (http://creativecommons.org/licenses/by/4.0/)

*Keywords:* Ammonia combustion; Carbon-free fuel; Energy carriers; NOx emission; Gas turbine

## 1. Introduction

The Paris Agreement on climate change was adopted at the Conference of Parties 21 (COP21) in 2015 [1] and aims to strengthen the global response

* Corresponding author.
*E-mail address:* kobayashi@ifs.tohoku.ac.jp (H. Kobayashi).

https://doi.org/10.1016/j.proci.2018.09.029
1540-7489 © 2019 The Authors. Published by Elsevier Inc. on behalf of The Combustion Institute. This is an open access article under the CC BY license. (http://creativecommons.org/licenses/by/4.0/)

to the threat of climate change by "holding the increase in the global average temperature to well below 2°C above pre-industrial levels and pursuing efforts to limit the temperature increase to 1.5°C above pre-industrial levels". This goal requires an extensive reduction in greenhouse gas (GHG) emissions and signatory nations are requested to show their own numerical goals for attaining this reduction, termed; Intended Nationally Determined Contribution (INDC). Combustion has been the main source of energy for human and industrial activities worldwide and efforts have been expended in the past to reduce GHG emissions via improved efficiency of combustion equipment. However, achieving the low emission targets requires the use of alternative carbon-free fuels in power generation and in industrial sectors that utilize combustion systems.

Most countries have defined their targeted reduction of GHG emissions for the future. The Japanese government, for example, set its INDC to be a 26.0% reduction in GHG emissions by fiscal year (FY) 2030 relative to recorded emissions in FY 2013 (a 25.4% reduction relative to recorded emission in FY 2005) [2]. The Japanese government have also set a reduction in GHG emissions target of 80% by FY 2050, as its long-term goal. In order to achieve the above targets, it is essential to replace a significant percent of fossil fuels with renewable energy sources. However, energy production from most renewable energy sources, such as wind, wave, tidal and solar is typically intermittent, thus storage of the energy in batteries or in chemical form is necessary in order to cushion the effects of fluctuation in energy production. Chemical storage, however, is more economical in comparison to batteries, and it also allows for the replacement of fossil-based fuels with carbon-free fuels, like hydrogen.

Hydrogen can be produced renewably from green energy sources via the electrolysis of water for example, and can be utilized in combustion systems, in fuel cells, and as a reagent in chemical synthesis. Recent advances in and increased utilization of renewable energy systems have been accompanied by a significant increase in hydrogen production and utilization, and international communities for investigating hydrogen production technology and utilization have been established to date. However, the economic storage and transport of hydrogen remain important unsolved challenges for its sustainable utilization, especially in countries and regions currently lacking natural gas pipelines which can be used to transport hydrogen mixed with natural gas. The adoption of the Kyoto Protocol, in 1997, at the Conference of Parties III (COP3) did not have a strong impact because developing countries did not undertake their obligations to meet the numerical targets for reducing GHG emissions [3]. Research and development of alternative means for hydrogen storage was intensified following COP3 leading to a consensus regarding the suitability of ammonia as a hydrogen and energy carrier.

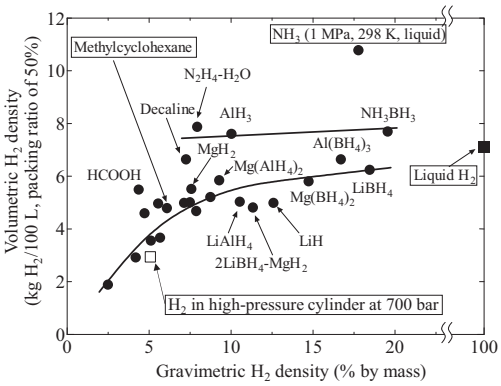


Fig. 1. Gravimetric and volumetric $H_2$ density of hydrogen carriers. Modified from [4].

### *1.1. Ammonia as a chemical compound and a hydrogen carrier in the energy and industrial sectors*

Figure 1 shows the gravimetric and volumetric hydrogen ($H_2$) densities for various hydrogen carriers. [4]. All candidate compounds other than pure hydrogen require energy to absorb and release hydrogen. Ammonia has a very high hydrogen density and can either be used as a fuel for combustion systems without requiring a hydrogen extraction process, or as a fuel in solid oxide fuel cells (SOFC) [5].

The process of manufacturing ammonia was invented about 100 years ago by F. Haber and C. Bosch. The process, which is best known as Haber-Bosch process, uses an iron-based catalyst at high pressure (100–300 atm) and high temperature (400–500°C) to combine hydrogen and nitrogen. Mass production of ammonia was started in 1913 by BASF. The major use of ammonia is for fertilizer in the agricultural sector, and it is reported to have allowed a drastic increase in food production to support a growing global population [6]. Ammonia is also used as a raw material for various industrial products, as well as a refrigerant in large-scale industrial coolers. Furthermore, ammonia is essential as a chemical additive for selective catalytic reduction (SCR) of NOx in thermal power generation, and most large-scale thermal power stations have installed ammonia tanks for that purpose. This well-established industry, more than 100 years old, of ammonia production, storage, transport and utilization makes it a suitable candidate to replace fossil-based fuels with minimal investment and with increased confidence due to familiarity and well-established processes.

Figure 2 shows a comparison of energy densities of a variety of fuels [7] as well as common batter-

Table 1
Thermal properties and fundamental combustion characteristics of ammonia and hydrocarbon fuels. Data of boiling point and condensation point are from NIST database [8].

| Fuel | $NH_3$ | $H_2$ | $CH_4$ | $C_3H_8$ |
|---|---|---|---|---|
| Boiling temperatureat 1 atm (°C) | −33.4 | −253 | −161 | −42.1 |
| Condensation pressure at 25 °C (atm) | 9.90 | N/A | N/A | 9.40 |
| Lower heating value, LHV (MJ/kg) | 18.6 | 120 | 50.0 | 46.4 |
| Flammability limit (Equivalence ratio) | 0.63∼1.40 | 0.10∼7.1 | 0.50∼1.7 | 0.51∼2.5 |
| Adiabatic flame temperature (°C) | 1800 | 2110 | 1950 | 2000 |
| Maximum laminar burning velocity (m/s) | 0.07 | 2.91 | 0.37 | 0.43 |
| Minimum auto ignition temperature (°C) | 650 | 520 | 630 | 450 |

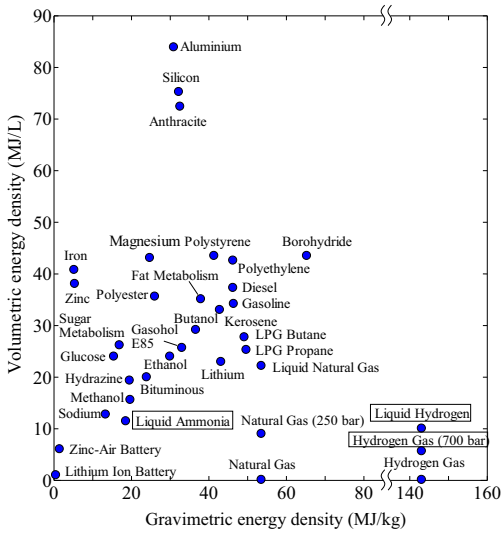


Fig. 2. Gravimetric and volumetric energy density of combustible materials and batteries. Higher heat value (HHV) for fuels are used because metals are included. Modified from [7].

ies. The higher heating value is used in the figure since some metals are included as well. The figure shows that the volumetric energy density of liquid ammonia is higher than that of liquid hydrogen and batteries, which is one of the qualities that make it attractive for energy storage and transport.

Table 1 contains a comparison of thermal properties and combustion characteristics of a variety of common gaseous fuels including methane, propane, hydrogen as well as ammonia. The table shows that the liquefaction of hydrogen requires a very low temperature of −252.9°C. Hydrogen storage at room temperature requires very high pressure. For example, a 700 atm hydrogen storage cylinder must be installed in fuel cell vehicles (FCVs) to have a range similar to that of vehicles using gasoline or diesel engines. Hence, high density hydrogen storage require substantial energy and costly storage equipment. On the other hand, the storage requirements of ammonia are similar to that of propane, with ammonia in liquid form at room temperature (25°C) when pressurized to 9.90 atm or temperature of −33.4°C at atmospheric pressure [8], indicating the higher potential of ammonia as both an energy and a hydrogen carrier.

About 180 M tons of ammonia are produced annually worldwide. At the present time, most commercial production of ammonia uses reformed hydrogen from natural gas or lignite and nitrogen separated from the air. It is estimated that the $CO_2$ emission from ammonia production plants is almost 1% of the total $CO_2$ released globally. Attempts to produce "green ammonia" using renewable hydrogen, as well as carbon capture and storage (CCS) for $CO_2$, are beginning in several regions, including Australia and Europe [9]. Furthermore, carbon capture, utilization and storage (CCUS) in which the separated $CO_2$ can be utilized as a chemical feedstock and for Enhanced Oil Recovery (EOR) makes $CO_2$ a valuable resource. Very recently, the International Energy Association (IEA) released a valuable report on strategies for renewable energy utilization in the industrial sector. The report concluded that ammonia is one of the most attractive energy carriers with significant economic advantages [10].

Since the boiling temperature and condensation pressure of ammonia are almost the same as those of propane (Table 1), transport ships designed for propane can generally be used for ammonia. Ammonia utilization as a fuel, however, has its drawbacks when compared to common hydrocarbon fuels. The heat of combustion of ammonia and the maximum laminar burning velocity of an $NH_3$/air flame are about 40% and 20%, respectively of those for typical hydrocarbon fuels as shown in Table 1. Furthermore, the flammability range for $NH_3$/air mixture is narrower and the ignition temperature is higher, indicating that ammonia has low flammability. Ammonia/air flame temperature is lower and radiation heat transfer from the flame is also lower than that of hydrocarbon flames because of the lack of $CO_2$ in the products. An additional challenge of $NH_3$/air combustion relates to the high fuel NOx emission. It is worth noting, however, that NOx is not a final product of ammonia combustion because the overall reaction of ammonia is $4NH_3 + 3O_2 \rightarrow 2N_2 + 6H_2O$ when con-

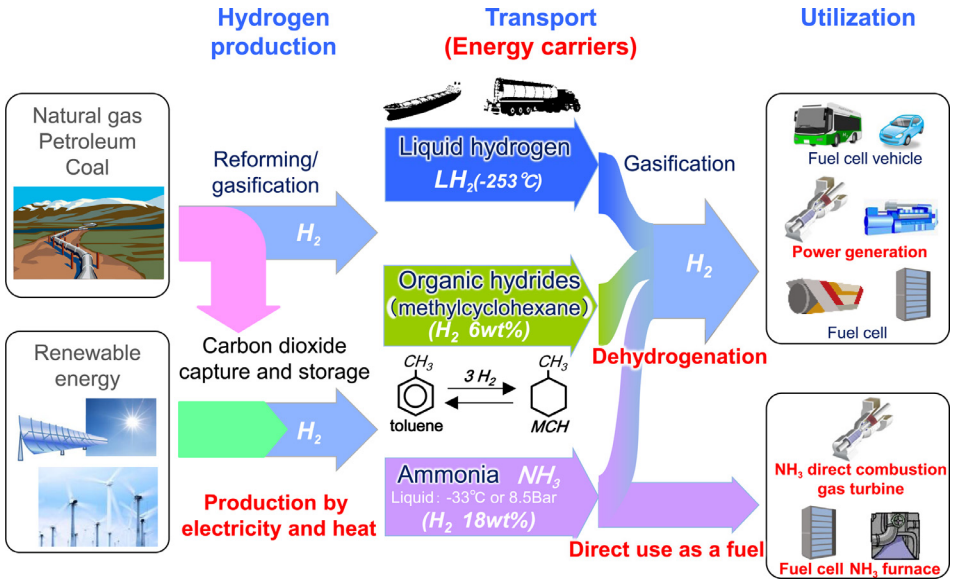


Fig. 3. Scheme showing hydrogen production, transport, and various uses [22]. Courtesy of Japan Science and Technology Agency (JST).

sidering the Gibbs free energy of the combustion products.

Despite these known challenges associated with ammonia as a fuel, attempts have been made to use ammonia as a fuel since the 1940s. During World War II, ammonia was added to coal gas which was used to drive the reciprocating engine of an omnibus [11]. In the 1960s, NASA's X-15 rocket-powered airplane used liquid ammonia and liquid oxygen, and achieved a world record for the highest manned flight Mach number of 6.7 [12]. In addition, the US Army had a research project to develop an ammonia-fuelled gas turbine but the project was not successful because of the very low combustion efficiency [13–15]. Ammonia has subsequently not been pursued as a fuel for combustion systems but has been used in combustion research to investigate NOx production and reduction chemistry, especially in the 1970s. The 1990s saw renewed interest in the utilization of ammonia as an energy source to address global warming, and research into ammonia utilization for reciprocating engines and gas turbines, especially using ammonia/hydrogen and ammonia/natural gas mixed fuels, have resumed [16–21].

### *1.2. Recent research and developments in ammonia fuel utilization in Japan*

Since the 1990s different national projects on hydrogen utilization have been funded in Japan, and in 2014 a new national project titled; "Cross-ministerial Strategic Innovation Promotion Program (SIP): Energy Carriers" was initiated [22].

The project includes subprojects for ammonia production using a new catalyst, the utilization of ammonia-dissociated hydrogen in a hydrogen station for FCV, as well as direct ammonia usage in gas turbines, reciprocating engines, industrial furnaces, and the co-firing of ammonia in pulverized coal combustion for power generation. Figure 3 shows a scheme for producing, transporting and using hydrogen in various ways.

In 2011, following the accident at the Fukushima nuclear power plant, all the nuclear power plants in Japan were shutdown. Since 2012, about 85% of the electricity in Japan has been generated by fossil fuel combustion. The low percentage of renewable energy generation in Japan relates to the small land area and high population density and contributes to more than 90% of the total energy needs of Japan being imported as fossil fuels from other countries. This situation will not change in the foreseeable future despite the requirement of reducing GHG emissions, and thus issues of hydrogen importation using a suitable storage medium has become increasingly important. Japanese energy organizations have determined that the three most promising hydrogen carriers are liquid hydrogen, organic hydrides (i.e., methyl cyclohexane), and ammonia. Studies of their transport to Japan and utilization are being performed [10].

Table 2 shows the properties of these three candidate energy carriers. It is clear that ammonia has significant advantages in terms of its direct utilization as a fuel in combustion systems and SOFC without dehydrogenation [5]. Three achievements

Table 2
Comparison of the properties of the three hydrogen carriers.

| Hydrogen carrier | $NH_3$ | Liquid $H_2$ | Methyl cyclohexane |
|---|---|---|---|
| Boiling temperatureat 1 atm (°C) | - 33.4 | −253 | 101 |
| Condensation pressureat 25 °C (atm) | 9.90 | N/A | 0.075 |
| Molecular weight | 17.0 | 2.02 | 98.2 |
| Hydrogen content (% by mass) | 17.8 | 100 | 6.16 |
| Hydrogen density (kg-H2/m3) | 121 | 70.8 | 47.3 |
| Energy to extract $H_2$(kJ/mol-$H_2$) | 30.6 | 0.907 | 67.5 |

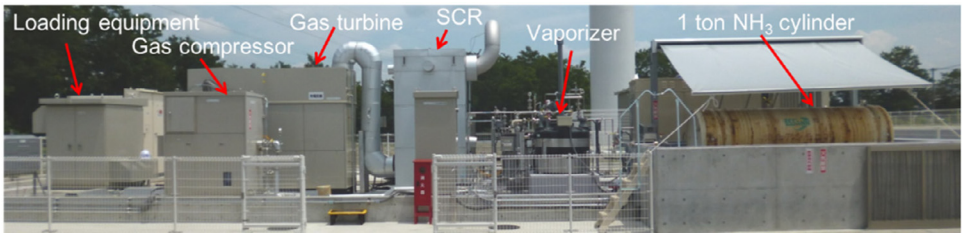


Fig. 4. Photo of the ammonia-fueled micro gas turbine test system at AIST [23]. Courtesy of the National Institute of Advanced Industrial Science and Technology, Japan (AIST).

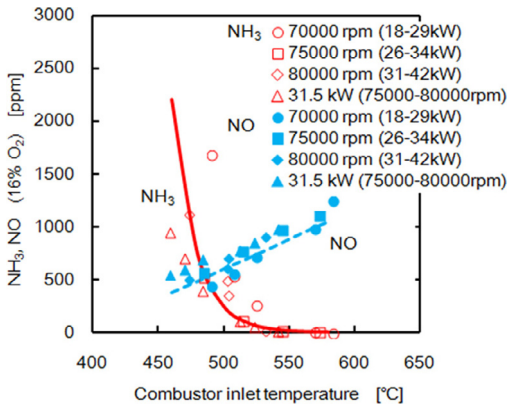


Fig. 5. The variation in NOx and $NH_3$ emissions at the combustor outlet with combustor inlet temperature for a single ammonia-fueled micro gas turbine. Modified from [24], courtesy of Dr. Osamu Kurata.

of the SIP project pertaining to ammonia combustion technology are described below.

The Fukushima Renewable Energy Institute of the National Institute of Advanced Industrial Science and Technology, FREA-AIST, succeeded in generating power using a micro gas turbine fuelled with ammonia/kerosene, ammonia/methane, and pure ammonia [24]. The gas turbine system uses a heat regenerative cycle to enhance the flame stability and combustion efficiency and consists of an $NH_3$ vaporizer, a gas compressor, and other components (Fig. 4). Figure 5 shows the variations of NOx and $NH_3$ emissions at the combustor outlet with combustor inlet temperature (CIT) for the micro gas turbine fueled with pure ammonia [24]. This combustor is a prototype originally designed to be operated on kerosene as a fuel and then modified to operate on ammonia by adding an ammonia injector. Therefore, an SCR system was installed downstream of the gas turbine to reduce the NOx concentration in the exhaust gas from about 1000 ppm to less than 10 ppm. When fuelled with either ammonia alone or ammonia/methane, 41.8 kW power generation was achieved. The combustion efficiency for a single fuelled ammonia operation was about 95%, and the residual $NH_3$ could be used as an additive for the SCR system. This prototype demonstrated that the CIT is the predominant parameter for emissions and combustion efficiency in gas turbine operation.

The Central Research Institute of Electric Power Industry, CRIEPI, performed experiments in ammonia co-fired pulverized coal combustion using a horizontal test furnace with a single burner [25]. Ammonia was injected into the furnace from several injection holes (Fig. 6) to test how NOx emissions varied with the geometric arrangement of the injection positions [25]. Results show that the maximum NOx emission did not increase with co-injection of ammonia into the furnace at ratios of more than 20% of the total LHV of the fuel. The location of the ammonia injection port influenced the level of NOx emissions as shown in Fig 7. For the case with an injection port 1.0 m downstream of the burner, NOx emission was found to be comparable to that of pulverized coal combustion without ammonia injection. This suggests that the injected ammonia behaved both as a selective non-catalytic reduction (SNCR) additive and as a fuel for heat release, indicating the significant potential of utilizing ammonia for pulverized coal

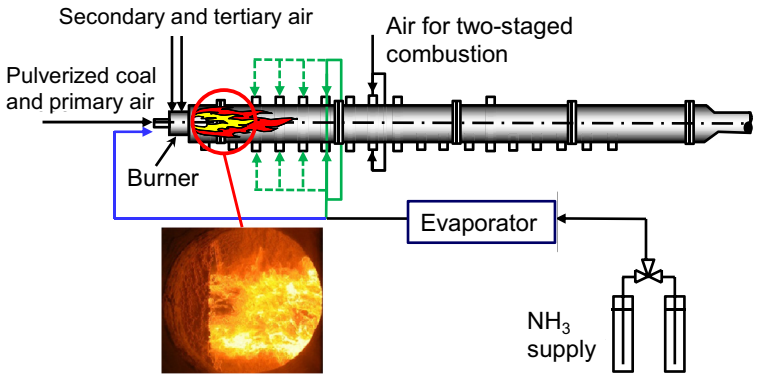


Fig. 6. Schematic of a horizontal pulverized coal furnace, and photo of the flame [25]. Courtesy of the Central Research Institute of Electric Power Industry, Japan (CRIEPI).

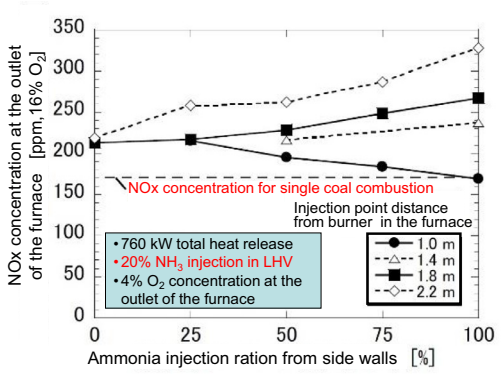


Fig. 7. NOx emission from the furnace and effect of the ammonia injection port [25]. Courtesy of the Central Research Institute of Electric Power Industry, Japan (CRIEPI).

combustion power generation to reduce GHG emission directly.

A group from Osaka University and Taiyo Nippon Sanso employed ammonia/natural gas (1:5 in LHV ratio) mixtures as fuel in a 10 kW scale test furnace using oxygen enriched air (30% $O_2$ maximum). A low NOx emission of less than 150 ppm at 11% $O_2$, a Japanese regulation standard, was attained by adjusting the secondary air injection port [26]. This experiment demonstrated the potential of ammonia utilization as a fuel for heat in industrial applications. Noteworthy, is that more than 20% of the energy consumed in industrial sectors is to generate heat, and thus the reduction of $CO_2$ emissions from industrial furnaces is another key approach for reducing GHG emissions by this sector.

Presented in the next section are fundamental characteristics of ammonia flames and combustion chemistry required to understand ammonia combustion in various applications and for further developing ammonia combustion technology.

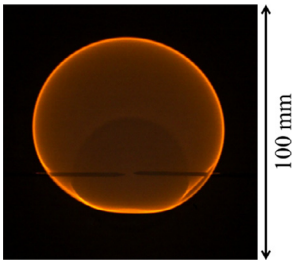


Fig. 8. A photograph of a spherically propagating $NH_3$/air laminar premixed flame at 0.10 MPa and mixture temperature of 298 K. Reprinted from [29] with permission from Elsevier.

## 2. Fundamentals of ammonia combustion and flame enhancement

### 2.1. Ammonia/air premixed flame characteristics

The fundamental flame characteristics of $NH_3$/air mixtures will be described in this section. Figure 8 shows an image of a spherically propagating $NH_3$/air laminar premixed flame. An orange flame is observed due to the $NH_2$ $\alpha$ band spectrum around 543.6–665.2 nm and the superheated water vapour spectrum [27,28].

Figure 9 shows experimental data of the unstretched laminar burning velocity, $S_L$, of $NH_3$/air premixed flames in terms of the equivalence ratio, $\phi$. The value of $S_L$ is maximum around $\phi = 1.1$. The maximum value of the laminar burning velocity of an $NH_3$/air premixed flame is about 7 cm/s, which is about 1/5 that of a $CH_4$/air flame [34]. The burnt gas Markstein length was obtained by Hayakawa et al. [29] and it increases monotonically with an

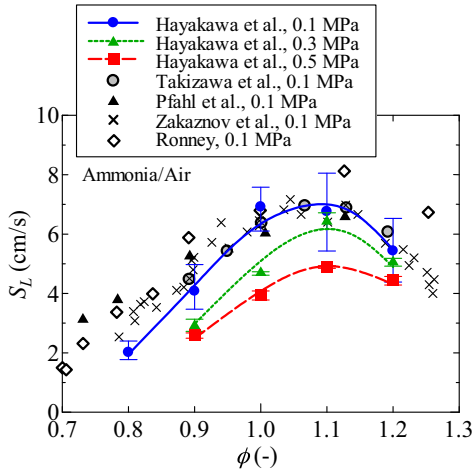


Fig. 9. Unstretched laminar burning velocity, $S_L$, of $NH_3$/air premixed flames in terms of equivalence ratio, $\phi$. The experimental results obtained by Hayakawa et al. [29], Takizawa et al. [30], Pfahl et al. [31], Zakaznov et al. [32] and Ronney [33] are plotted. Mixture temperature = 298 K. Reprinted from [29] with permission from Elsevier.

increase in the equivalence ratio. The trend of the Markstein length with respect to $\phi$ is the same for $H_2$/air [35] and $CH_4$/air flames [36], and interestingly is opposite that for iso-octane/air flames [36].

The Lewis number of an $NH_3$/air flame is slightly lower than unity for a lean mixture, and the burnt gas Markstein length is negative for $\phi \leq 0.9$. The value of the burnt gas Markstein length decreases when the pressure increases from 0.1 MPa to 0.3 MPa, while the change is smaller when the pressure increases from 0.3 MPa to 0.5 MPa.

### 2.2. Comparisons of flame characteristics between ammonia/air and methane/air mixtures

The features of $NH_3$/air premixed flames are discussed below in comparison with $CH_4$/air premixed flames. Figure 10 shows a comparison of the structures of $NH_3$/air and $CH_4$/air premixed flames at an equivalence ratio, $\phi$, of 1.0 and a pressure, $P$, of 0.1 MPa. The detailed reaction mechanism developed by Mathieu and Petersen [37] was employed for the unstretched one-dimensional (1D) simulation of $NH_3$/air flames, while GRI Mech 3.0 [38] was employed for that of $CH_4$/air flames. Note that the scales on the abscissa for the $NH_3$/air and $CH_4$/air flames are different. The volumetric heat release rate of the $NH_3$/air flame is lower than that of the $CH_4$/air flame. The flame thickness of $NH_3$/air premixed flame is larger than that of the $CH_4$/air premixed flame because of the lower burning velocity of $NH_3$/air mixture. The flame thickness calculated from the temperature profiles and shown in Fig. 10 are 2.85 mm and 0.44 mm for $NH_3$/air and $CH_4$/air flames, respectively. Another

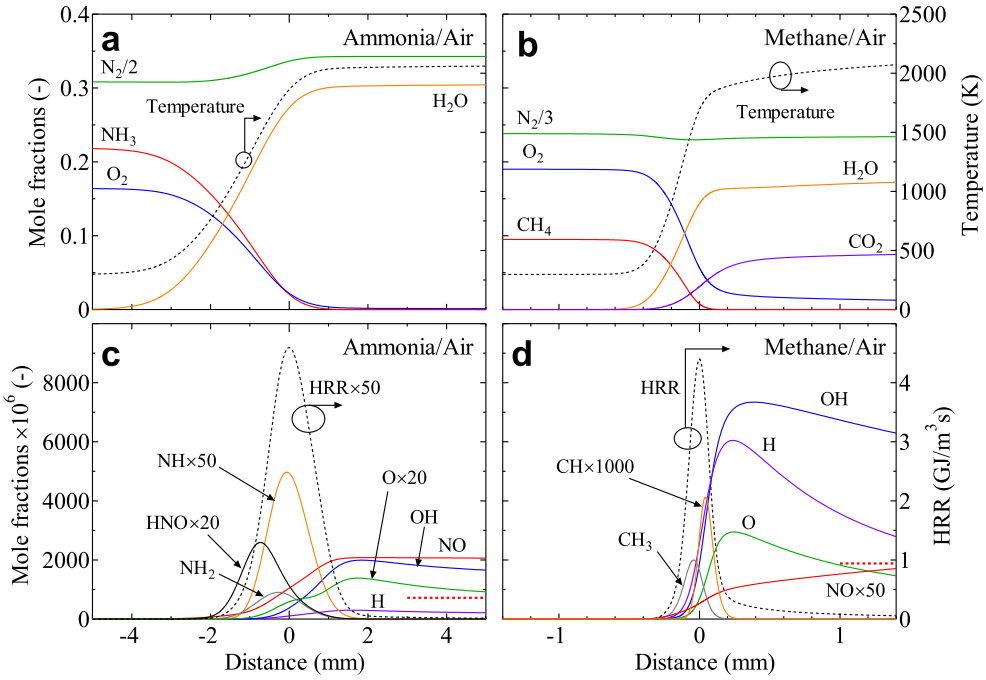


Fig. 10. Flame structures of $NH_3$/air ((a) and (c)) and $CH_4$/air ((b) and (d)) premixed flames at $\phi = 1.0$ and $P = 0.1$ MPa. The thick red broken lines in (c) and (d) represent the mole fraction of NO at equilibrium.

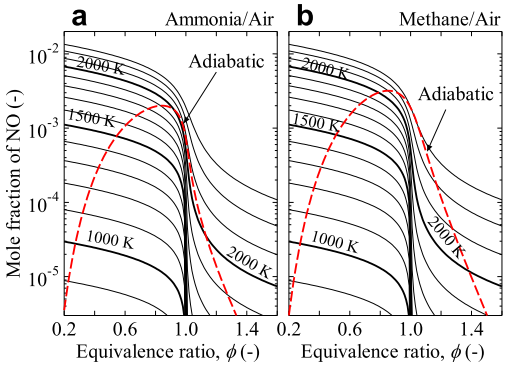


Fig. 11. Variation in the NO mole fraction at equilibrium at given temperatures and adiabatic flame temperatures, with equivalence ratios: (a) $NH_3$/air; (b) $CH_4$/air.

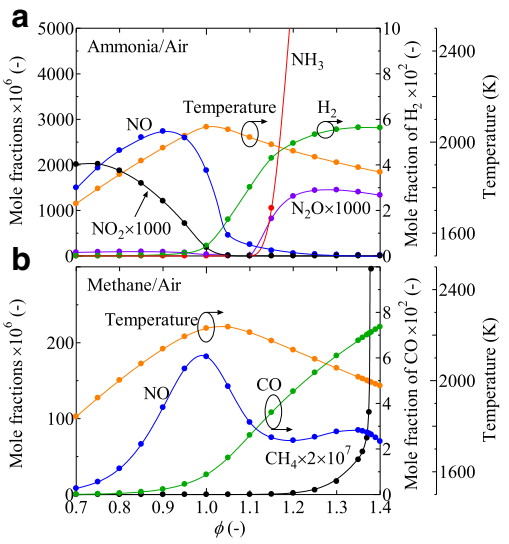


Fig. 12. Emission characteristics in terms of equivalence ratio at 0.1 MPa and 40 mm downstream of the position of maximum heat release rate: (a) $NH_3$/air; (b) $CH_4$/air.

important feature is the NO profile across the flames. Since NO is generated mainly through the fuel NO pathway in ammonia flames, the NO concentration rapidly increases in the reaction zone and gradually decreases away from this zone [27]. In the case of a $CH_4$/air flame, however, the NO concentration increases gradually in the post-flame zone because NO is mainly produced thermally via the Zeldovich mechanism. The thick red broken lines in Fig. 10c and d represent the NO mole fraction at equilibrium. The NO mole fraction at equilibrium in $NH_3$/air flame at $\phi = 1.0$ and $P = 0.1$ MPa is lower than that of $CH_4$/air flame.

Figure 11 shows the NO mole fractions at chemical equilibrium of $NH_3$/air and $CH_4$/air flames and at 0.1 MPa. The NO mole fraction of $NH_3$/air flames at adiabatic conditions was lower than that of $CH_4$/air flames. At the exit of an actual combustor, however, the NO concentration from an $NH_3$/air flame is likely higher than that from a $CH_4$/air flame because of the finite scale of the combustor.

Estimating NO emission characteristics using equilibrium calculations is insufficient for realistic evaluation of the NO concentration in an ammonia flame and thus the emission characteristics were evaluated from unstretched 1D flame simulations. Figure 12 shows the mole fractions of chemical species in the product gas 40 mm downstream of the position of maximum heat release rate. The NO mole fraction of $NH_3$/air flames is much higher than that of $CH_4$/air flames and the value obtained by equilibrium calculation. The reduction of NO for rich mixtures will be discussed in Section 3. $NO_2$ and $N_2O$ are also plotted in Fig. 12 because these species are important contributors to total NOx. However, the mole fractions of $NO_2$ and $N_2O$ are low when compared to NO. Therefore, NO reduction is the main challenge to achieving low-NOx combustion in $NH_3$/air premixed flames. The amount of unburnt $CH_4$ in the product gas from a rich $CH_4$/air flame is very low, but the mole fraction of unburnt $NH_3$ rapidly increases in rich $NH_3$/air flames. Hence, there is a trade-off in the relationship between NO and unburnt $NH_3$ emission, and simultaneous NO and $NH_3$ emission reduction is therefore required in order to use ammonia as a fuel. The total emission of NO and $NH_3$ reaches a minimum around $\phi = 1.1$ and the use of this slightly rich condition can simultaneously reduce NO and $NH_3$. In addition, a rich mixture is relatively high in $H_2$ and is useful for two-stage combustion in an ammonia-fueled gas turbine combustor. Details of the two-stage combustion of ammonia are described in Section 4. The maximum temperature of $NH_3$/air flames is about 100–200 K lower than that of $CH_4$/air flames at the same equivalence ratio.

Figure 13 shows a comparison of experimental values of extinction limits, $\varepsilon_{ext}$, of $NH_3$/air and $CH_4$/air obtained from counter flow twin flames in terms of $\phi$. Here, Tian's mechanism [41] and GRI Mech 3.0 [38] were employed for the $NH_3$/air and $CH_4$/air flames, respectively. The extinction limits of the $NH_3$/air flames are lower than those of the $CH_4$/air flames. However, Colson et al. [39] clarified that the relative rate of increase in extinction limits with pressure of ammonia flames is larger than that of methane flames, and this observation was discussed from the standpoint of the characteristic time of the reaction. For $NH_3$/air flames, the decrease in the characteristic time of the reaction is more significant than that of $CH_4$/air flames and causes a significant increase in the extinction limit of ammonia flames at elevated pressure.

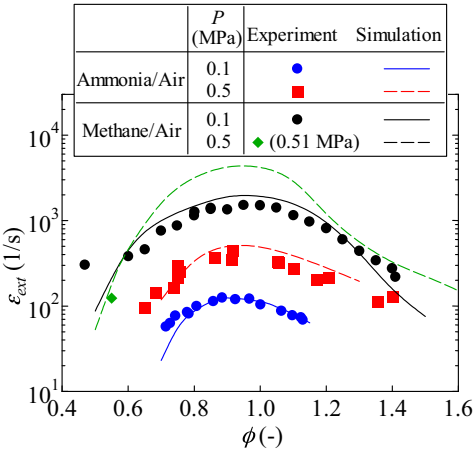


Fig. 13. Extinction flame stretch rate, $\varepsilon_{ext}$, in terms of equivalence ratio, $\phi$. The experimental values for the extinction limits of $NH_3$/air and $CH_4$/air flames were acquired by Colson et al. [39] and Takita et al. [40], respectively. All simulations were performed by Colson et al. [39]. Mixture temperature = 298 K.

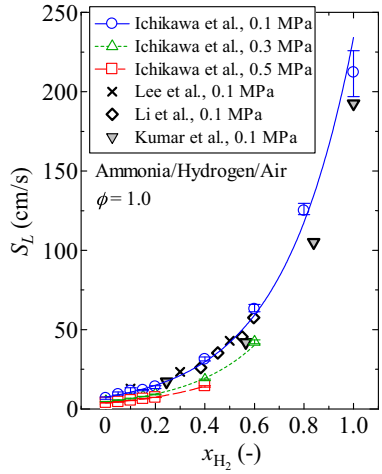


Fig. 14. Relationship between laminar burning velocity and volumetric hydrogen fraction in the binary fuel of ammonia and hydrogen. The values obtained by Ichikawa et al. [42], Lee et al., [43], Li et al. [44] and Kumar et al. [45] are plotted. Mixture temperature = 298 K.

From the above discussion, it can be concluded that $NH_3$/air premixed flames are less stable than $CH_4$/air flames exhibiting lower laminar burning velocities, heat release rates, flame temperatures, and extinction stretch rates.

### 2.3. Flame enhancement of ammonia/air flames

The low burning velocity of $NH_3$/air flames make flame enhancement important for the successful application of ammonia as a fuel. Hydrogen addition is a reasonable approach for simultaneously achieving carbon-free combustion and flame enhancement. Figure 14 shows the change in laminar burning velocity with hydrogen addition. Here, the abscissa, $x_{H2}$, represents the volumetric hydrogen fraction in the binary fuel comprising ammonia and hydrogen. Because of the high reactivity of hydrogen, the laminar burning velocity exponentially increases with $x_{H2}$, and the laminar burning velocity becomes the same order of magnitude as that of a $CH_4$/air flame at around $x_{H2} = 0.4$.

Mørch et al. [46] and Frigo and Gentili [16] studied the application of $NH_3/H_2$ fuel in spark ignitions engines. Robust engine cycles were promoted with an increase in hydrogen content in the fuel, and the minimum hydrogen-to-ammonia energy ratio for robust engine operation was reported to be approximately 7% at full load and 11% at half load [16]. Hydrogen addition was also attempted in a gas turbine-like combustor by Valera-Medina et al. [20]. Since hydrogen can be easily produced by the thermal decomposition of ammonia, additional hydrogen storage is not required when a $NH_3/H_2$ mixture is employed as a fuel. Comotti and Frigo [47] employed a ruthenium-based catalyst to produce hydrogen from ammonia and used it to operate a spark ignition engine.

Blending ammonia with conventional hydrocarbon fuels results in fuels of higher flame speeds, heat release rate and radiation intensity than ammonia, and of lower $CO_2$ emission than the hydrocarbon. Ammonia-blended hydrocarbon fuels are also important from the viewpoint of a stepwise shift towards a carbon-free society.

There has been a couple of fundamental studies on the combustion characteristics of ammonia-blended hydrocarbon fuels. Henshaw et al. [48] and Okafor et al. [49] measured the laminar burning velocities of flames of $CH_4/NH_3$ fuel mixtures for different equivalence ratios. Figure 15 shows the decrease in the laminar burning velocities of $CH_4$/air flames with an increase in $NH_3$ concentration, measured as $E_{NH3}$ which represents the heat fraction of $NH_3$ in the binary fuel of $CH_4/NH_3$. Zietz and Baumgärtel [50] and Bockhorn et al. [51] measured the laminar burning velocities of flames of $C_3H_8/NH_3$/air mixtures and again show the decrease in burning velocity with an increase in $NH_3$ concentration. Emission characteristics of $CH_4/NH_3$/air flames were measured by Henshaw et al. [48], Jójka and Ślefarski [52] and Valera-Medina et al. [18]. Even though only up to 4 - 5% of $NH_3$ by volume was added to $CH_4$, NO concentration in the exhaust increased by several orders of magnitude reaching unacceptable levels of 4000 ppm at the burner exit [48,52].

Application of ammonia-blended hydrocarbon fuels in internal combustion engines have also been studied. Numerical studies have shown the

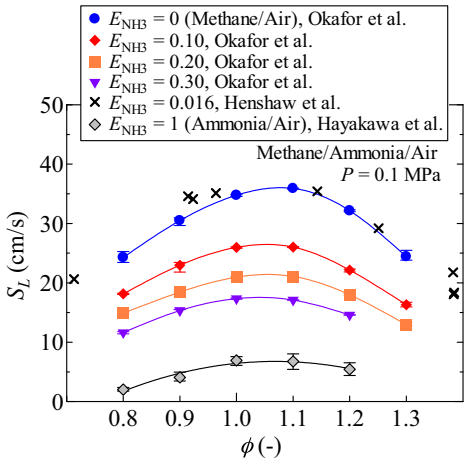


Fig. 15. Variation of the unstretched laminar burning velocity with ammonia addition in $CH_4$/air flames. The laminar burning velocities obtained by Henshaw et al. [48] and Okafor et al. [49] are plotted. The laminar burning velocities of $NH_3$/air flames are also plotted for reference [29]. Mixture temperature and pressure were 298 K and 0.10 MPa, respectively.

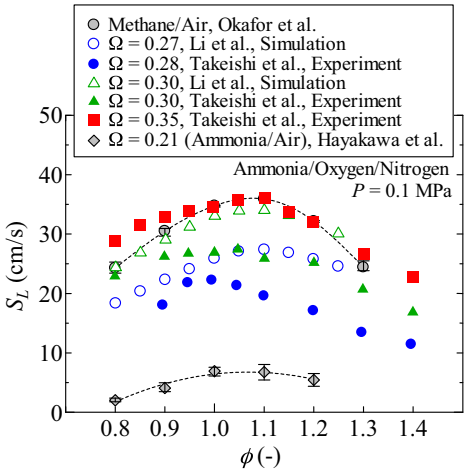


Fig. 16. Variation of laminar burning velocity of oxygen-enriched $NH_3/O_2/N_2$ flames in terms of equivalence ratio. The experimental results obtained by Takeishi et al. [55] and the numerical results obtained by Li et al. [56] are plotted. The laminar burning velocities of $CH_4$/air and $NH_3$/air flames are also plotted for reference [29,49]. Mixture temperature and pressure were 298 K and 0.10 MPa, respectively.

potential of application of diesel-ammonia dual fuels in compression ignition engines [53,54]. Valera-Medina et al. [18] studied the combustion of $CH_4/NH_3$/air pre-mixture in a swirl combustor up to 0.2 MPa for various equivalence ratios. Unstable flame behavior was observed when the $NH_3$ concentration in the fuel increased to 70-80 mol.%, while the mixture could not be ignited when the $NH_3$ concentration increased to 90 mol.%. Kurata et al. [24] demonstrated the generation of power using a gas-turbine fuelled with pure $NH_3$ or $NH_3/CH_4$ as discussed Section 1. The results show that $NH_3/CH_4$ mixtures resulted in a wider operating power range, and higher combustion and thermal efficiencies than $NH_3$/air mixtures due to the enhancement of ammonia combustion by methane addition. HCN emission of about 20 ppm was recorded at low operating power conditions of 15 kW where the level of unburned $NH_3$ emission was about 60 ppm. However, with complete combustion of ammonia at high operating power conditions, HCN emission was negligible.

Another approach to increase flame burning velocity is to augment the oxidant stream through oxygen enrichment. Takeishi et al. [55] measured the laminar burning velocity of ammonia flames from a slot burner for various oxygen concentrations in the oxidant stream as shown in Fig. 16. Here, Ω represents the $O_2$ concentration in the $O_2/N_2$ mixture. These experimental results show that the laminar burning velocity approaches that of $CH_4$/air flames when the $O_2$ concentration in the $O_2/N_2$ mixture was 0.35, a mixture ratio commonly used in oxygen-enriched industrial furnaces.

Ammonia-oxy flames have also been widely studied. Andrews and Gray [57] and Armitage and Gray [58] evaluated the laminar burning velocity and flammability limits of $NH_3/O_2$ mixtures. The flame structure of $NH_3/O_2$ was studied by Maclean and Wagner [59], Bian et al. [60], and Lindstedt et al. [61]. The NO formation characteristics of $NH_3/O_2$ were examined by Setchell and Miller [62]. The flame temperature increases with increased oxygen addition, improving the weak radiation characteristics of ammonia flames. Murai et al. [63] examined the heat transfer characteristics of ammonia flames by radiation using a 10 kW test furnace and showed that the heat flux at $\Omega = 0.3$ is higher than that of $CH_4$/air flames. Therefore, oxygen-enriched ammonia flames are useful in improving the heat transfer characteristics of ammonia flames, as stated in Section 1.

Turbulence leads to wrinkling and stretching of the flame front, consequently increasing the turbulent flame surface density and flame speed relative to the laminar one. Mixing is also enhanced by turbulence. The first study of turbulent ammonia flames was performed by Rohde et al. [64]. Because of the low flammable characteristics of ammonia, Rohde et al. focused on flame stability. As mentioned in Section 2.1, the laminar burning velocity is smaller and the preheating zone thickness larger than those of conventional hydrocarbon flames. For instance, the relative chemical time scales i.e., the ratio of the flame thickness to the unstretched laminar burning velocity for stoichiometric $CH_4$-air and $NH_3$-air flames at 298 K and 0.10 MPa are

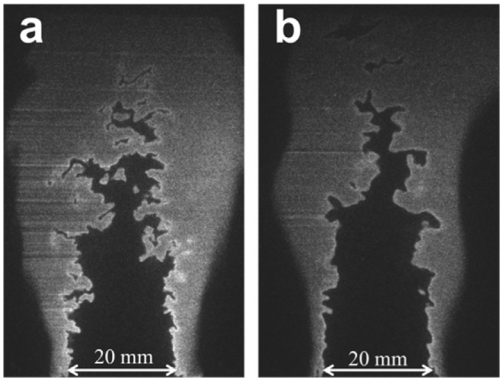


Fig. 17. OH-PLIF images of turbulent flames at 0.5 MPa and mixture temperature of 298 K ($u'/S_L \approx 4.7$): (a) $CH_4$/air flame; (b) $CH_4/NH_3$/air at $E_{NH3} = 0.3$.

1.2 ms and 41.3 ms, respectively. Therefore turbulent $NH_3$/air premixed flames can exhibit significantly high turbulence Karlovitz numbers and have higher tendency to be in the broken reactions zones regime of the Peters diagram [65]. The characteristics of ammonia turbulent flames thus may give insight into the structure of flames in this regime which has attracted the interest of the turbulent combustion community (e.g., [66]).

Figure 17 shows OH-PLIF images of $CH_4$/air and $CH_4/NH_3$/air premixed turbulent flames for $\phi = 0.9$ around $u'/S_L \approx 4.7$. The finest scale of the flame front wrinkles seems to be larger in the case of the $CH_4/NH_3$/air mixture. The change in flame front structure is presumably caused by an increase in the preheating zone thickness by ammonia addition.

## 3. Chemical kinetics of ammonia oxidation and fuel NOx

Ammonia oxidation chemistry has been extensively studied over the past several decades mainly because of its relevance to fuel NOx formation and selective non-catalytic reduction of NOx (SNCR) using ammonia as a reducing agent [67–70]. Detailed reviews of this oxidation chemistry can be found in the literature [71–74]. Hence, only a brief discussion is provided here below.

Among the important early efforts to describe ammonia oxidation with detailed kinetics are the work of Miller and co-workers. [72,75,76]. Miller et al. [76] investigated computationally a variety of burner-stabilized and freely propagating $NH_3/O_2$ and $NH_3/H_2/O_2$ flames and proposed detailed kinetics of $NH_3$ oxidation with 22 species and 98 elementary reactions. At lean and moderately rich conditions, their model satisfactorily predicts the species profiles measured by MacLean and Wagner [59], Green and Miller [77], Fenimore and Jones [78], and the burning velocity measured by Murray and Hall [79]. The model, however, fails to predict the measurements satisfactorily at rich flame conditions, and this was attributed to the ammonia pyrolysis mechanism being incomplete.

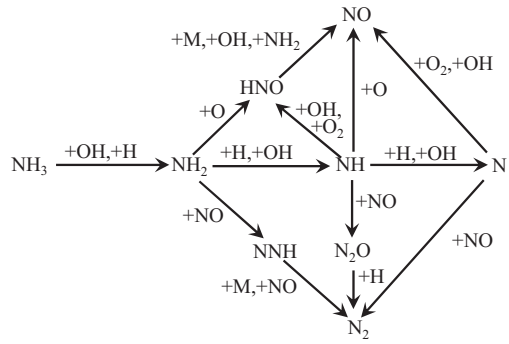


Fig. 18. $NH_3$ oxidation pathway by Miller et al. Reprinted from [76] by permission of Taylor & Francis Ltd.

The understanding of ammonia oxidation has improved since the pioneering works by Miller and co-workers and the kinetics models have improved in comprehensiveness and accuracy over the years. Nevertheless, the reaction pathway proposed by Miller et al. [76], as shown in Fig. 18, remains relevant to understanding the chemistry of $NH_3$ oxidation, and fuel NO formation and reburn, as discussed below.

### 3.1. Lean ammonia flame kinetics

Ammonia is consumed by H abstraction primarily through the reaction with OH under all conditions of equivalence ratio. Other secondary consumption steps include the reactions with H and O, with $NH_2$ being the common product. $NH_i$ ($i = 0, 1, 2$) oxidation may primarily lead to NO formation, mainly through an HNO intermediate, or to NO reduction through $NH_i + NO$ reactions, depending on the concentration of the O/H radicals. The abundance of O/H radicals favors the conversion of $NH_i$ to NO, and may inhibit the reduction of NO by $NH_i$ radicals, as discussed in more detail in Section 3.4. Because O/H radicals are abundant in lean flames, with a peak around the equivalence ratio of 0.9, lean ammonia flames have high NO concentration which peaks around the equivalence ratio of 0.9 as shown in Fig. 12a. Skreiberg et al. [80] noted that the addition of CO to lean $NH_3/NO/O_2/N_2$ flames at 1273 K increased the O/H radical pool, resulting in an increase in NO production via the HNO route. On the other hand, Mendiara and Glarborg [81] observed that the addition of $CO_2$ to stoichiometric $NH_3/CH_4$/air flames resulted in a significant decrease in NO production due to depletion of the O/H radical pool as the $CO_2$ consumed H atoms to form CO.

HNO is primarily produced through the reaction of $NH_2$ with O atoms. The NH→HNO path constitutes a secondary route for HNO production. HNO is then solely oxidized to NO. Recent kinetics studies show that HNO is converted to NO in the flame mainly through reactions with H, OH, $O_2$, and through thermal dissociation. The HNO intermediate channel is the dominant NO production path in $NH_3$/air flames under all conditions.

Following the studies of Miller et al. [76], Bian et al. [82] studied lean and stoichiometric $H_2/O_2$/Ar premixed flat flames doped with $NH_3$ or $NH_3 + NO$ at low pressure using molecular beam mass spectrometry. They recorded relatively low HNO concentrations and concluded that HNO is not relevant in fuel NO production. They therefore excluded all HNO reaction steps in their simplified $NH_3$ oxidation mechanism and proposed that NO is primarily produced via the reactions of $NH_i$ ($i = 1, 2$) with $O_2$. Later studies, such as those of Lindstedt et al. [61,83], however, affirmed the dominance of the HNO channel in fuel NO production. Lindstedt et al. [61] studied a set of flat laminar premixed $NH_3/H_2/O_2$, $NH_3/NO/H_2/O_2$ and $NH_3/O_2$ flames by detailed chemical kinetic modelling and developed a comprehensive kinetics model, which was validated using the species profiles measured by Bian et al. [82], Vandooren et al. [84], and MacLean and Wagner [59]. Lindstedt et al. [61] reported that for lean $H_2/O_2$ flames doped with $NH_3$ or $NH_3 + NO$, about 70% of the NO is produced through the HNO channel. Their detailed mechanism was systematically reduced to 7, 5 and 4-step mechanisms whose prediction of the species profiles in the flame have considerably close agreement with the detailed model [83].

### 3.2. Rich ammonia flame kinetics

The O/H radical concentration decreases as the flame becomes richer but the relative concentration of H in the O/H radical pool in the flame increases. This increases the tendency for $NH_i$ ($i = 1$, 2, 3) to be oxidized through reactions with H atoms, leading to substantial $H_2$ production mainly from $NH_2$, and ultimately to the production of N atoms. The relative abundance of N atoms in rich flames promotes the set of reactions known as the extended Zeldovich mechanism, as discussed in Section 3.3.

The lower concentration of O/H radicals in rich ammonia flames leads to lower NO production from $NH_i$ oxidation. This may explain the lower NO concentration at rich conditions, as shown in Fig. 12a. In addition, the promotion of $NH_i$ combination reactions in rich flames contributes to lower NO production from the $NH_i$ radicals [69,76,86]. Haynes [69] studied routes for NO formation and reduction in ammonia flames and suggested that $N_2$ formation through $NH_i + NH_i$ reactions may be relatively greater in richer lower temperature flames where $NH_3$ is more stable. Subsequent studies by Dean et al. [86] found that $NH_i$ combination reactions dominate the kinetics of rich ammonia flames and contribute to the low NO production. Reactions of the type $NH_i + NH_i$ provide an alternative route for $NH_i$ conversation to $N_2$ without involving NO, mainly through the path $NH_2 \xrightarrow{+NH_2,\,NH} N_2H_2 \xrightarrow{+M,\,H} NNH \xrightarrow{+M,\,O,\,O_2} N_2$. NNH consumption is primarily through the dissociation reaction, while the reactions with O and $O_2$ are secondary.

Dean and Bozzeli [73] proposed that NNH may lead to substantial NO production through the so-called NNH mechanism, which involves the reaction of NNH with an O atom. This suggests that a substantial amount of NO may result from the $NH_i$ combination pathway. The reaction of NNH with an O atom has three product channels: $NNH + O = NH + NO$, $NNH + O = N_2O + H$, and $NNH + O = N_2 + OH$. Dean and Bozzeli [73] conducted a QRRK analysis and reported that the rate constants of the $NH + NO$ and the $N_2O + H$ channels are about one order of magnitude larger than that of the $N_2 + OH$ channel. Subsequently, a number of kinetic modeling studies have associated a substantial amount of NO production to the NNH mechanism in hydrogen [87–89] and hydrocarbon flames [90–92]. However, Konnov and co-workers [93,94] and Klippenstein et al. [95] proposed that the rate constant of the $NH + NO$ channel may be significantly smaller than the value proposed by Dean and Bozzeli [73]. Klippenstein et al. [95] analyzed theoretically reactions on the $NNH + O$, $NNH + O_2$ and $NH_2 + O_2$ potential energy surfaces in order to elucidate the role of NNH in NO formation and showed that of the three $NNH + O$ product channels, the $N_2 + OH$ channel is dominant while the $N_2O + H$ channel is competitive. The $NO + NH$ channel was found to be a relatively minor channel even at high temperatures due to the endothermicity of the reaction.

Konnov and De Ruyck [96] recognized that the formation of $N_2H_3$ and $N_2H_4$ from $NH_i$ radical combination steps was neglected in earlier studies, such as those of Miller and Bowman [72], Vandooren et al. [84], and Lindstedt et al. [61]. The authors [96] therefore included the reactions of these species in their detailed N/H mechanism. A comparison of their modelling results with measurements of ammonia pyrolysis in shock waves by Davidson et al. [97] showed that addition of the $N_2H_i$ reactions resulted in more satisfactory prediction of the rise-time and peak concentrations of NH and $NH_2$ radicals. However, the prediction deviates significantly from the measurements at temperatures above about 2800 K. Several versions and updates of Konnov's mechanism have since then been reported [87,98–102]. Duynslaegher et al. [103] proposed a modification of the rate con-

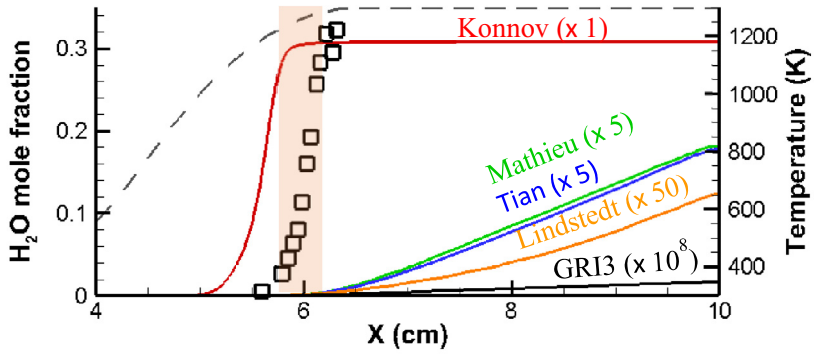


Fig. 19. Measured (symbols) and computed (solid lines) species profiles of $H_2O$ of weak ammonia flames in a micro flow reactor with a controlled temperature profile. Modified from [104].

stants of four reactions to improve the prediction of $NH_2$ and $N_2O$ profiles by Konnov's mechanism.

Recent studies by Nakamura et al. [104,105] showed that among the mechanisms proposed by Lindstedt et al. [61], Konnov et al. [101], GRI Mech 3.0 [38], Tian et al. [41], and Mathieu and Petersen [37], only Konnov's mechanism predicts the formation of weak $NH_3$/air flames in Nakamura et al.'s micro flow reactor experiments, as shown in Fig. 19. Tian's mechanism [41] describes in detail $CH_4/NH_3$ oxidation kinetics, validated with measured species profiles of $NH_3/CH_4/O_2/Ar$ stoichiometric flames at 4 kPa using tuneable synchrotron vacuum ultraviolet photoionization and molecular-beam mass spectrometry. The N/H/O subset is based on the kinetics of Skreiberg et al. [80]. On the other hand, Mathieu's mechanism [37] provides detailed hydrocarbon/$NH_3$ kinetics validated with ignition delay time measurements behind the reflected shock waves over a wide range of conditions for mixtures of ammonia highly diluted in argon. The $NH_3$ subset was drawn from the kinetics of Dagaut et al. [106]. Nakamura et al. [104,105] attributed the better performance of Konnov's mechanism to its superior representation of $N_2H_i$ chemistry, which is important in low temperature ammonia oxidation. The authors then developed a detailed $NH_3$ kinetics model, based on the kinetics described by Miller and Bowman [72] with updates from Konnov's mechanism [101] and Mathieu's mechanism [37]. This detailed model was validated using measurements of weak flames, ignition delay times, and burning velocity [105].

### 3.3. Extended Zeldovich mechanism in ammonia combustion

One important NO production route from the combustion of nitrogen-free fuels in air is the thermal-NO mechanism, usually referred to as the extended Zeldovich mechanism, involving $N_2 + O = NO + N$, $N + O_2 = NO + O$ and $N + OH = NO + H$. The first reaction is the rate-limiting reaction for this mechanism and requires cleavage of the covalent N–N bond in $N_2$. Consequently, it is favored at high temperatures, typically above 1800 K. Therefore, for hydrocarbon fuels and even low-nitrogen-containing fuels such as natural gas in which the extended Zeldovich mechanism is the main contributor to NOx formation, temperature control is the most important factor in NOx control [73].

In ammonia flames, however, the extended Zeldovich mechanism is active even at low temperatures, although its net contribution to NO concentration may be negligible. Figure 20 shows the percent contribution of each step of the mechanism to the total rate of NO production (positive values) or reduction (negative values) in $NH_3$/air flames. The rate of NO production is integrated over the entire computation domain for each elementary reaction. Note that $N_2 + O = NO + N$ is a reduction step for NO in ammonia flames because the abundance of NO and N atoms favors the backward reaction. All the kinetics models, except GRI Mech 3.0, show that the importance of the extended Zeldovich mechanism is promoted in rich flames. In the models of Miller [76] and Konnov [102], $N_2 + O = NO + N$ is the primary NO reduction step in rich flames, and these kinetics models predict that the net influence of the extended Zeldovich mechanism in rich $NH_3$/air flames is a reduction of NO. The predictions made by Okafor's mechanism [49], which is a detailed $CH_4/NH_3$ oxidation kinetics model based on GRI Mech 3.0 with the addition of important N/H chemistry from Tian's mechanism, agrees with that of Tian's mechanism, as shown in Fig. 20.

An increase in temperature enhances the O/H radical pool due to promotion of the temperature-sensitive chain branching reactions. Consequently, total NO production and reduction increases and decreases, respectively. However, the net

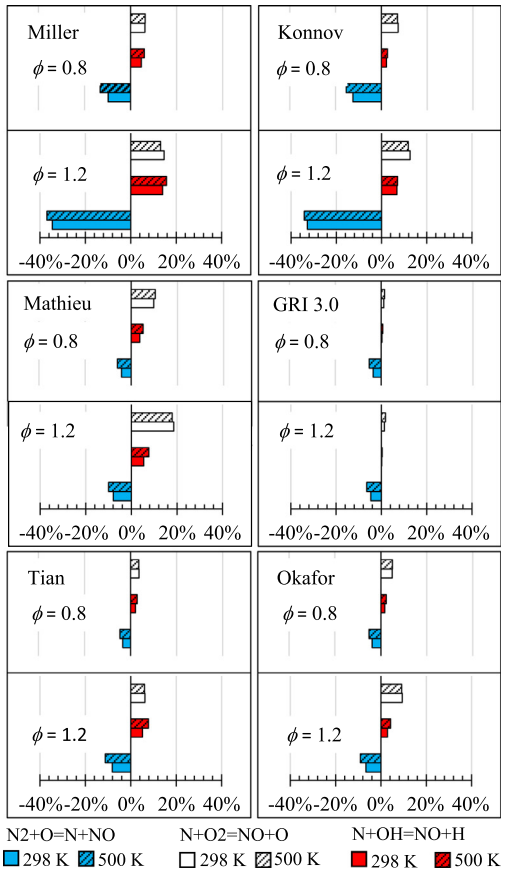


Fig. 20. Percent contribution of the extended Zeldovich mechanism to total NO production or reduction in $NH_3$/air flames at different initial mixture temperatures.

contribution of the extended Zeldovich mechanism to NO concentration may not be significantly affected by temperature. As shown in Fig. 20, the rates of NO reduction via $N_2 + O = NO + N$ and production via $N + OH = NO + H$ increase with temperature, while NO production via $N + O_2 = NO + O$ does not respond significantly to an increase in temperature.

### 3.4. NO reduction kinetics

The reaction of NO with $NH_i$ ($i = 0, 1, 2$) leads to the reduction of NO to $N_2$. These reactions take place under all conditions but are promoted under particular conditions. The reaction of NO with N atoms, as discussed in the previous section, is promoted in rich flames and at elevated temperatures. NO reduction by NH primarily produces $N_2O$ via $NH + NO = N_2O + H$. $N_2O$ is then largely consumed through $N_2O + H = N_2 + OH$ [85]. The dominant NO reduction step under all conditions, especially in lean flames, is the reaction of NO with $NH_2$, which has two product channels, $NH_2 + NO = NNH + OH$ - (R1) and $NH_2 + NO = N_2 + H_2O$ - (R2).

Lyon [67,68] found that within a certain temperature range and oxygen concentration, NOx reduction in flames can be enhanced using $NH_3$ in a process called Thermal DeNOx. Studies by Miller et al. [75] and a host of subsequent studies [72,76,95,107–109] explained that the $NH_2 + NO$ reactions are key to the thermal DeNOx process. The self-sustaining character of the DeNOx mechanism is due to the direct or indirect production of OH and O from R1 at a rate controlled by the branching ratio, $\alpha = k_1/(k_1 + k_2)$, and the lifetime of NNH. NNH promotes the production of OH and O through the steps $NNH = N_2 + H$, $H + O_2 = O + OH$, and $O + H_2O = OH + OH$. The smaller the branching ratio, the slower the chain-branching R1 relative to the chain terminating R2. Consequently, there is increased tendency to hinder the production of O/H radicals, which sustains the conversion of $NH_3$ to $NH_2$ for a continuation of NO reduction. On the other hand, a large $\alpha$ may result in substantial promotion of O/H radical production, given the very short lifetime of NNH ($10^{-11}$ to $10^{-8}$ s) proposed by theoretical studies [110–114]. Consequently, conversion of $NH_2$ to NO rather than NO reduction may be favored [74]. The sensitivity of the thermal DeNOx process to the concentration of O/H radicals contributes to its dependence on temperature. At the lower boundary of the effective thermal DeNOx temperature window, the chain terminating reaction $H + O_2 + M = HO_2 + M$ competes with $H + O_2 = O + OH$ and hence inhibits the thermal DeNOx process. On the other hand, above the upper temperature boundary, there is significant growth in the O/H radical pool, leading to net NO production rather than reduction. It can thus be understood that the NO formation/reduction in ammonia flames, as well as the reactivity of the N/H/O chemistry, may be significantly dependent on $\alpha$ and the lifetime of NNH. Nakamura et al. [105] concluded that $\alpha$ is a key parameter controlling ammonia reactivity.

There have been several efforts to accurately evaluate $\alpha$ [61,72,107,108,115–120]. Miller and Bowman [72] noted that for the thermal DeNOx process to be self-sustaining, $\alpha$ must be at least 0.25 at the lower boundary of the temperature window. They proposed an optimum value of $\alpha = 0.508$, with a relatively long NNH lifetime of $10^{-4}$ s. Miller and Bowman [72] considered that the very short lifetime of NNH proposed by theoretical studies implies that the product of the chain branching channel, R1, is $N_2 + H + OH$, which contradicts experimental observations that show OH, rather than H, to be a direct product of the $NH_2 + NO$ reaction [121–124]. More recent experimental [108,115,118,119] and theoretical [61,107,116,117,120] studies, however, indicate

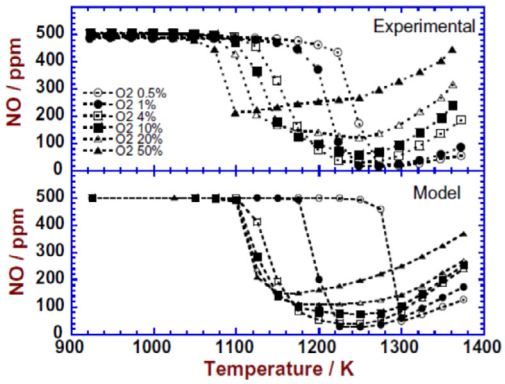


Fig. 21. Modeling of the effects of temperature and $O_2$ on the thermal DeNOx by Klippenstein et al. [95]. The experiment is from Kasuya et al. [109]. Inlet concentrations: $NH_3 = 1000 \pm 60$ ppm, $NO = 500 \pm 30$ ppm, $H_2O = 5\%$, balance $N_2$. Residence time (s) = 88.0/T(K). The reactor surface/volume ratio was 7.8 $cm^{-1}$. Reprinted from [95] with permission from Elsevier.

that $\alpha$ may be temperature dependent, with a value smaller than 0.508 within the thermal DeNOx temperature window. Klippenstein et al. [95] adopted a very short NNH lifetime of $10^{-9}$ s in their model, and $\alpha(T)$ proposed by Miller and Klippenstein [120] which ranges from 0.3 to 0.4 within the temperature range of 1100 K to 1400 K. Their predictions of the dependence of the thermal DeNOx process on temperature and $O_2$ concentration agree closely with the measurements by Kasuya et al. [109], as shown in Fig. 21. However, the lower temperature boundary is over-predicted by their mechanism for $O_2$ concentrations above 4% due to the very short NNH lifetime.

### 3.5. Effects of pressure on ammonia flame chemistry

The primary consumption step for ammonia remains essentially unaltered as pressure increases, even though the O/H radical pool is depleted with an increase in pressure. The three-body pressure-sensitive reactions $H + OH + M = H_2O + M$ and $H + O_2 + M = HO_2 + M$ are promoted with an increase in pressure. The former reaction is a chain terminating reaction while the latter competes with the production of OH from $H + O_2$ and produces less active $HO_2$ radicals. This reduction of the active O/H radical pool results in a decrease in NO production. Hayakawa et al. [27] showed that the concentration of NO in stoichiometric $NH_3$/air flames has a high negative sensitivity to the rate constant of $H + OH + M = H_2O + M$, which increases appreciably with pressure.

In addition, the consumption of $NH_i$ via the radical combination steps may be promoted as pressure increases and further contribute to a decrease in NO production, as discussed in Section 3.2. Konnov's mechanism predicts that the rate of the addition reactions of $NH_i$, such as $NH + NH + M = N_2H_2 + M$, $NH_2 + NH_2 + M = N_2H_4 + M$, and $NH_2 + NH + M = N_2H_3 + M$, are enhanced with an increase in pressure. Song et al. [125] noted that the reaction $NH_2 + NH_2 + M = N_2H_4 + M$ constitutes a minor $NH_2$ consumption step at 10 MPa. However, in Skreiberg's mechanism [80] and most other kinetic mechanisms derived from it, these reactions are not modeled as pressure-dependent three body reactions.

It is worth noting that this kinetics of $NH_i$ combination reactions which produce $N_2H_i$ species has not yet been well characterized despite evidence of its importance in rich and low temperature ammonia flames [86,104,105]. The kinetics of $N_2H_i$ reactions is excluded in Mathieu's mechanism [37], however, the mechanism models several characteristics of ammonia oxidation satisfactorily as discussed in the next section, Section 3.6.

### 3.6. Validation of ammonia oxidation kinetics

Despite the vast number of studies on ammonia oxidation kinetics, wide disparities still exist in the prediction of ammonia combustion characteristics by different kinetics mechanisms. With kindled interest in ammonia as a fuel, there is need for more work on the optimization and validation of kinetics models over a wider range of relevant conditions. This has motivated several recent measurements of ignition characteristics [37,104,105], burning velocity [29,42,45,49], and the extinction stretch rate [39] of ammonia and ammonia-blended mixtures, as discussed in Section 2. Furthermore, there are growing efforts to validate the kinetics mechanisms at, for instance, gas turbine-relevant conditions [126,127].

Figure 22 compares the measured ignition delay times of Mathieu and Petersen [37] with predictions made by selected kinetics models. Dagaut's mechanism [106] and Mathieu's mechanism [37] provide the most satisfactory predictions of the measurements. However, the reactivity of ammonia could be over-predicted by most kinetics mechanisms, such as those of Hughes, Mueler, Mével, Duynslaegher, Konnov and Miller, which under-predict the ignition delay times.

Figure 23 shows that Mathieu's mechanism also predicts the unstretched laminar burning velocity of $NH_3$/air flames satisfactorily while those of Konnov and Miller over-predict the burning velocity. Tian's mechanism agrees well with the measurements shown in Fig. 23 at lean conditions, but over-predicts them at rich conditions. Tian's mechanism was reported by Kumar et al. [45] to predict the burning velocity of ammonia/hydrogen flames more satisfactorily in comparison to Konnov's mechanism and GRI Mech 3.0. However, Tian's

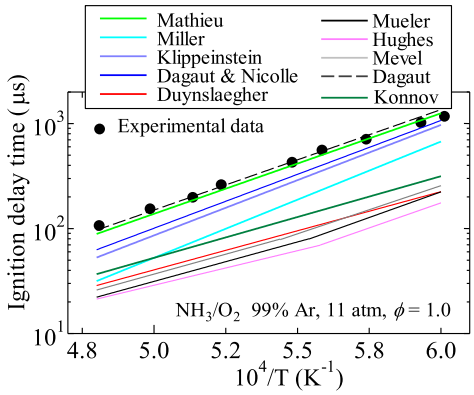


Fig. 22. Comparison of the ignition delay measurements of Mathieu and Petersen [37] with prediction by selected kinetics models: Mathieu [37], Miller [72], Konnov [98], Duynslaegher [103], Dagaut [106], Klippenstein [95], Mueller [128], Hughes [129], Dagaut and Nicole [130], and Mével [131]. Modified from [37].

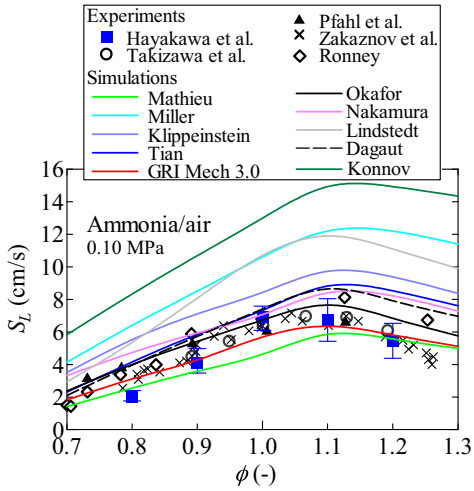


Fig. 23. Comparison of the measured burning velocity to predictions made by the kinetics models of Mathieu [37], Okafor [49], Miller [76], Lindstedt [61], Konnov [102], Nakamura [105], Tian [41], Dagaut [106], GRI Mech 3.0 [38], and Klippenstein [95]. Mixture temperature and pressure were 298 K and 0.10 MPa, respectively.

mechanism significantly under-predicts the burning velocity of $CH_4/NH_3$/air mixtures due mainly to the dominance of HCO (+ H, OH, $O_2$) = CO (+ $H_2$, $H_2O$, $HO_2$) over HCO = CO + H in the conversation of HCO to CO in the kinetics [49].

GRI Mech 3.0 is seen to closely predict the measurements shown in Fig. 23 but lacks some important ammonia oxidation steps, such as the $NH_i$ radical combination reactions and the $NH_2 + NO$ reactions. These sets of reactions are not important in flames with trace quantities of ammonia, such

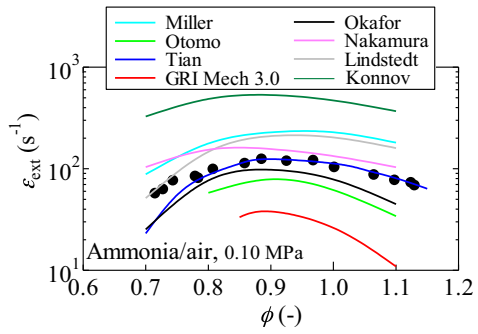


Fig. 24. Comparison of the measured extinction stretch rate by Colson et al. [39] with predictions made by the kinetics models of Okafor [49], Miller [76], Lindstedt [61], Konnov [102], Nakamura [105], GRI Mech 3.0 [38], Tian [41], and Otomo [132]. Mixture temperature = 298 K.

as natural gas, but are important, particularly for prediction of the NO concentration, in flames of fuels with high ammonia concentration [49].

Using Okafor's mechanism [49] it is possible to predict the laminar burning velocity of $NH_3$/air flames satisfactorily at all equivalence ratios, model the burning velocity of $CH_4/NH_3$/air flames satisfactorily [49], and to predict the structure of $CH_4$/air flames in accordance with that of GRI Mech 3.0. However, since Okafor's mechanism describes $NH_3$ kinetics more comprehensively, it has a higher potential to model $NH_3$-containing flames more satisfactorily than GRI Mech 3.0.

As shown in Fig. 24, Tian's mechanism and Okafor's mechanism give the closest predictions of the extinction stretch rate of $NH_3$/air flames. GRI Mech 3.0 significantly under-predicts the measured data while Konnov's mechanism substantially over-predicts it.

The mechanisms of ammonia oxidation in flames are quite different from those of ammonia ignition because the O/H radical pool in the flame is much larger than that generated during the induction period of ignition. In addition, $N_2H_i$ chemistry, which was found to dominate ammonia ignition chemistry [105], is less important in the flames. Nevertheless, the rate of production of O/H radicals predicted by a kinetics mechanism may affect its prediction of the ignition and flame characteristics of ammonia mixtures. A consistent pattern can be found in the prediction of the ignition delay time, burning velocity, and extinction stretch rate by several of the kinetics models above. The mechanisms of Konnov and Miller, for instance, consistently over-predict the measured properties, suggesting an over-prediction of ammonia reactivity. These "over-reactive" kinetics mechanisms predict relatively higher rates of production of O/H radicals than most other kinetics models and thus they may also over-predict the NO concentration in ammonia flames.

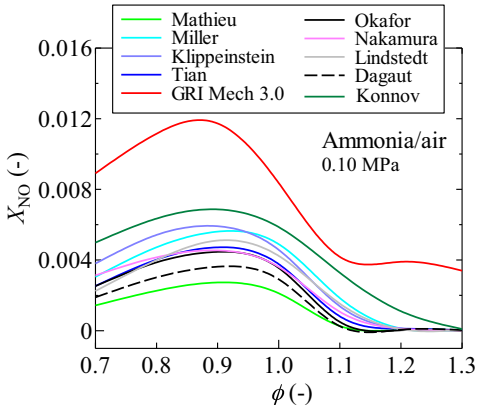


Fig. 25. Comparison of the predicted NO concentration 4 cm downstream of the point of maximum heat release made by the kinetics models of Mathieu [37], Okafor [49], Miller [76], Lindstedt [61], Konnov [102], Nakamura [105], GRI Mech 3.0 [38], Tian [41], Dagaut [106], and Klippenstein [95].

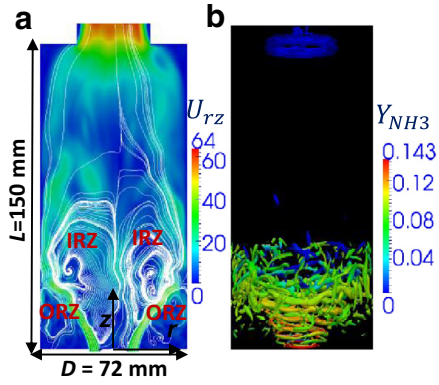


Fig. 26. Instantaneous reacting flow field of turbulent non-premixed $NH_3$/air flames at $\phi = 1$ and $P_0 = 0.1$ MPa: (a) streamlines and two-dimensional velocity distribution in a vertical plane; (b) iso-surfaces of the second invariant of the velocity tensor, $Q$ of $3 \times 10^7$ (as median value), shaded with mass fraction of $NH_3$, $Y_{NH3}$. (Numerical Codes: OpenFOAM, Model: LES, Sub-grid Scale Model: wall adaptive local eddy-viscosity ( WALE) model, mean inlet velocity, $U_{in}$= 39.1 m/s, swirl number = 0.68) [133]. Courtesy of Japan Society of Mechanical Engineers.

Figure 25 shows that, with the exception of GRI Mech 3.0, the mechanisms of Konnov and Miller predict the highest concentrations of NO in the post flame. The NO prediction by GRI Mech 3.0 is about twice that of most other kinetics models because of its incomplete $NH_3$ oxidation chemistry. The prediction of NO concentration by Tian's mechanism, Nakamura's mechanism and Okafor's mechanism agree quite well. It has been shown by Xiao et al. [126] that Tian's mechanism predicts NOx emissions from gas turbine combustors fired with a mixture of 40% methane and 60% ammonia by volume more satisfactorily in comparison to GRI Mech 3.0 and Konnov's mechanism [101], as well as Mendiara's mechanism [81], which was developed based on Tian's mechanism.

## 4. Emissions abatement from an ammonia-fueled gas turbine combustor

### *4.1. Numerical analysis of a model gas-turbine-like combustor with detailed ammonia chemistry*

In hydrocarbon combustion, the use of lean premixed flames is one of the most promising gas turbine combustion techniques employed to meet the strict legislative limits on combustion pollutant emissions. However, lean turbulent premixed flames, which are characterized by lower burning velocities relative to stoichiometric flames, lead to combustion instability. A commonly used way of stabilizing lean premixed flames is by employing swirling flow which creates an inner recirculation with a low velocity zone, and thus enhances flame anchoring. Moreover, the recirculation continuously supplies hot burnt gases and active radicals to the fresh unburned mixture.

Recent numerical and experimental studies on turbulent premixed $NH_3$/air flames by Somarathne et al. [133,134] and Hayakawa et al. [135], respectively, showed that the recirculating flow upstream of the combustor, as shown in Fig. 26a, results in stable combustion of turbulent premixed $NH_3$/air flames under high turbulent intensity and pressure conditions. Apparent in Fig. 26a are two distinct recirculation zones, namely; inner recirculation zones (IRZ) associated with lower static pressure near the bottom center of the combustor created by swirling flows, and outer recirculation zones (ORZ) created due to the sudden expansion of the reacting flows in the combustion chamber. Moreover, rotational flow structures downstream of the swirler, as shown in Fig. 26b, are generated by means of iso-surfaces of the second invariant of the velocity gradient tensor, Q, of $3 \times 10^7$, chosen as a median value. Using LES to conduct three-dimensional (3D) numerical studies [133,134], the authors reported that fuel NO generation can be significantly reduced by using rich flame conditions at high pressure, as shown in Fig. 27a. This reduction is due to the significant decrease in OH radicals in rich ammonia flames and at high pressures, as shown in Fig. 27b. Miller's mechanism [76] for ammonia oxidation was used in these numerical studies. The promotion of $NH_i$ radical combination paths in rich flames and at high pressure can contribute to the significant decrease in fuel NO concentration, as discussed in Sections 3.2 and 3.5. Moreover, numerical studies [133,134] and an experimental

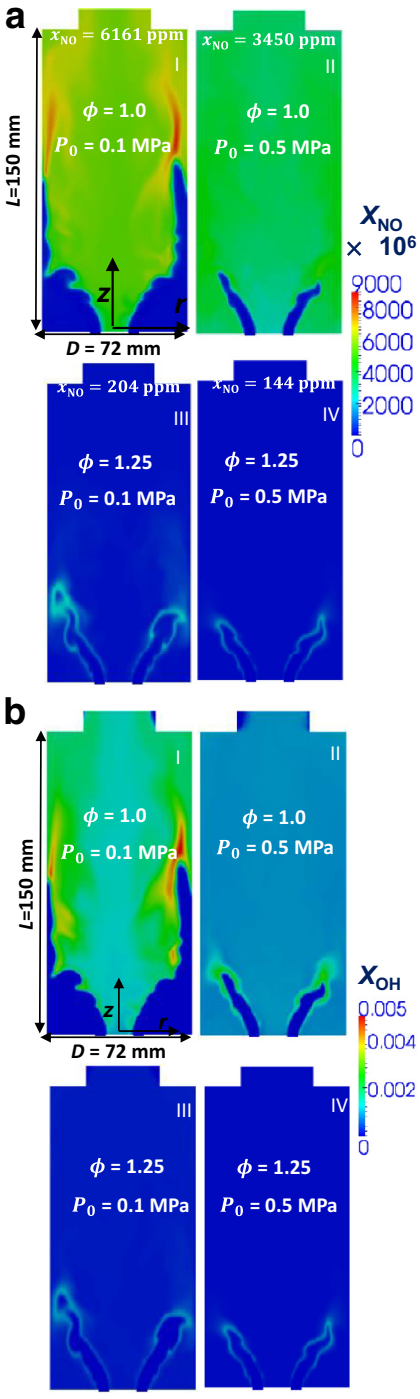


Fig. 27. (a) NO; (b) OH; concentration distributions in turbulent premixed $NH_3$/air flames in terms of e quivalence ratio, $\phi$, and pressure, $P_0$ (at an inlet temperature, $T_0$, of 500 K, mean inlet velocity, $U_{in}$= 39.1 m/s, swirl number = 0.68. Combustor walls are adiabatic) Reprinted from [134] with permission from Elsevier.

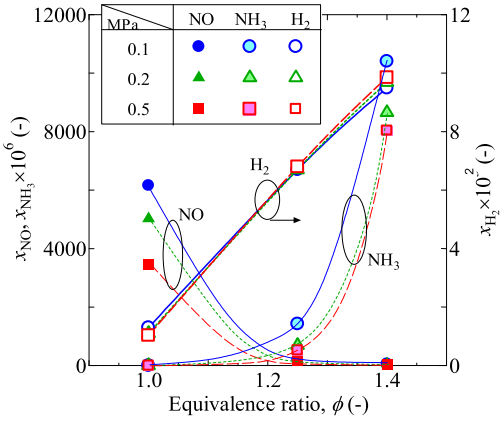


Fig. 28. Space and time averaged emissions of NO, $x_{NO}$, $NH_3$, $x_{NH3}$, and $H_2$, $x_{H2}$ in turbulent premixed $NH_3$/air flames in terms of equivalence ratio, $\phi$, and pressure, $P_0$ (at an inlet temperature of 500 K). Reprinted from [134] with permission from Elsevier.

studies [135,137] verified that there is a specific equivalence ratio, $\phi_{sp}$, in rich flame conditions (at every pressure condition) at which NO and unburnt $NH_3$ emissions are minimal and that the emissions followed the same order as shown in Fig. 28. These results again verify the emission characteristics of 1D $NH_3$/air flames discussed earlier in Section 2.2. The studies described in [133],[134] showed that $\phi_{sp}$ was 1.2 when the mixture inlet temperature was 500 K using an adiabatic wall condition. On the other hand, an experimental study [135] found that $\phi_{sp} = 1.05$ for a mixture temperature of 300 K and using an isothermal combustor wall condition.

Hence, it was confirmed that a slightly rich condition gives minimum NO and $NH_3$ emissions regardless of flame configuration and 3D simulation successfully estimates the emission characteristics of ammonia combustion.

In addition, the same study [133] showed that the effect of pressure on unburnt $NH_3$ emission is also significant, such that at $\phi_{sp}$=1.2, an increase in pressure from 0.1 MPa to 0.5 MPa leads to a reduction in $NH_3$ emission from 700 ppm to 200 ppm mole fraction. This unburnt $NH_3$ emission decrease is due to a significant decrease in the characteristics time of the chemical reaction in $NH_3$/air flames with an increase in pressure, which leads to an increase in overall Damköhler number.

The emission characteristics of turbulent non-premixed $NH_3$/air flames were numerically examined [136]. The results showed that even though NO emission decreased with an increase in the global equivalence ratio, $\phi_{global}$, similar to premixed flames, the distribution of NO concentration within the combustor was non-uniform, unlike in the premixed flame case, as shown in Fig. 29a. The NO concentration in the center

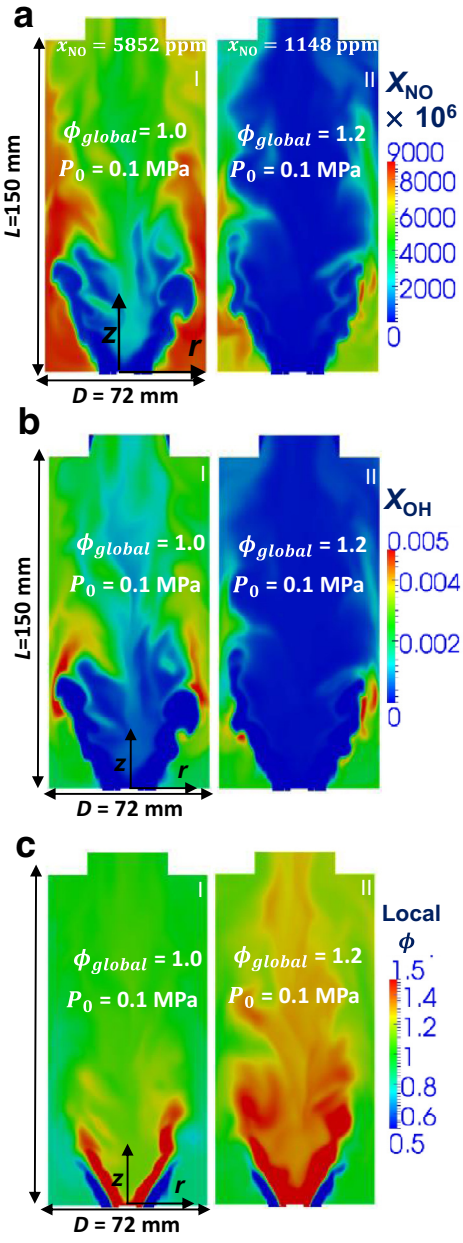


Fig. 29. (a) NO; (b) OH; and (c) local $\phi$; distributions in turbulent non-premixed $NH_3$/air flames in terms of equivalence ratio, $\phi$ (the fuel and air stream inlet temperatures are 500 K and the swirl numbers are 0.69 and 0.68, respectively. Combustor walls are adiabatic). Reprinted from [136] by permission of Taylor & Francis Ltd.

region of the combustor was zero but high NO concentration zones appeared near the combustor wall boundaries, irrespective of $\phi_{global}$. This behavior may be related to the non-uniformity of OH concentration within the combustor, as shown in

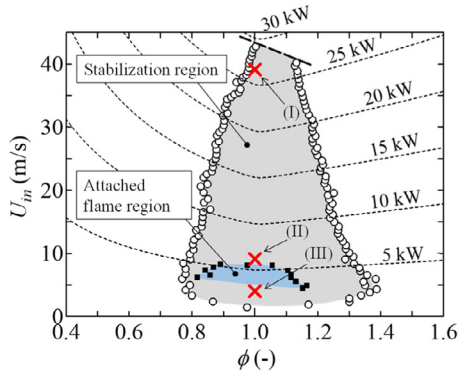


Fig. 30. Stabilization limits shown on a mean inlet velocity, $U_{in}$, and equivalence ratio, $\phi$, map. The dotted lines represent heat values calculated using an equilibrium calculation (at an inlet temperature of 300 K and a pressure of 0.1 MPa).

Fig. 29b, which is related to the local $\phi$ distribution within the combustor, as shown in Fig. 29c.

### 4.2. Experimental study of $NH_3$ premixed flames stabilized on a model swirl burner

Figure 30 shows the flame stabilization limit map obtained using the same swirler and combustor configurations as used for premixed $NH_3$/air flames. The symbol ○ represents the stability limit obtained experimentally for an inlet mixture temperature of 300 K and a pressure of 0.1 MPa. Figure 30 shows that $NH_3$/air can be stabilized over a wide range of $U_{in}$ and $\phi$, without the need for any additives.

The maximum $U_{in}$ can be increased to more than 40 m/s, and the maximum heat release from the burner exceeded 25 kW. The broken line near the condition I in Fig. 30, denotes an upper limit imposed by the experimental setup. However, the flame is expected to also stabilize above this limit. The flame stabilization $\phi$ range is between 0.75 and 1.40 at $U_{in}$= 5 m/s, and these limits are close to the lean and rich flammability limits of 0.63 and 1.40, respectively, for $NH_3$/air flames (Table 1) [34]. As $U_{in}$ increases, the flame stabilization $\phi$ range narrows, and this narrowing is related to the laminar burning velocity characteristics over equivalence ratio range in Fig. 9. A lower flame stabilization limit is observed at $U_{in}$= 1.8 m/s, which means that a certain minimum swirling motion is required for $NH_3$/air flame to stabilize. Worth noting, is that flames can also be stabilized in the ORZ under certain operating conditions. In Fig. 30, the stabilization limits of these flames, which are referred to as attached flames, are represented by the square symbol, ■.

Figure 31 shows photographs of the flames taken under the three conditions specified in Fig. 30. The sets of $U_{in}$ and $\phi$ at these three

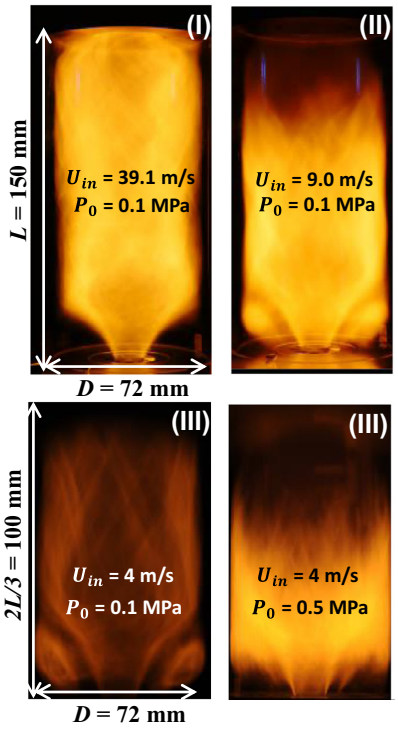


Fig. 31. Photographs of the flames at $U_{in}$ and $\phi$ of I (39.1 m/s, 1.0), II (9.0 m/s, 1.0), and III (4 m/s, 1.0) (at $P_0$ values of 0.1 and 0.5 MPa and combustor inlet temperature of 298 K).

conditions respectively are I (39.1 m/s, 1.0), II (9.0 m/s, 1.0), and III (4.0 m/s, 1.0). Moreover, at condition III, a flame image was also taken at $P_0 = 0.5$ MPa. The flame height is proportional to the inlet velocity of the mixture. Importantly, an increase in pressure leads to a reduction in flame height, as discussed in Section 4.1, and is associated with the significant decrease in the characteristic time of chemical reaction with an increase in pressure.

### 4.3. Two-stage combustion for low NOx ammonia/air combustors

Somarathne et al. [134] described the effects of secondary air injection on the ultimate emission characteristics of NO, unburnt $NH_3$, and $H_2$ from $NH_3$/air premixed flames. The report suggested that the equivalence ratio, $\phi_{pri}$, of the primary combustion zone should be at $\phi_{sp}$, corresponding to minimal NO and unburnt $NH_3$, in order to achieve overall minimum NO emission with zero $NH_3$ and $H_2$ emissions, as shown in Figs. 32 and 33. Under richer conditions, there is essentially no NO generation in the primary combustion zone, but unburnt $NH_3$ from the primary combustion zone enters into

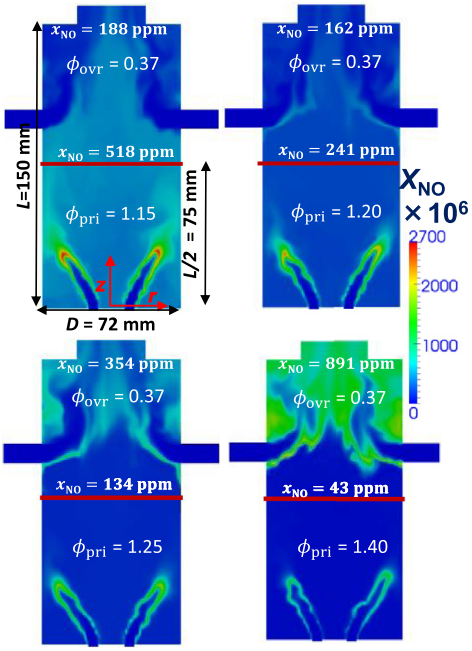


Fig. 32. Effect of secondary air injection on overall NO emission in terms of $\phi_{pri}$ at $P_0 = 0.5$ MPa. Reprinted from [134] with permission from Elsevier.

the secondary combustion zone. This results in the generation of NO again in a lean combustion environment, as shown in Fig. 32, and thus leading to high NO emission.

### 4.4. Development of a low NOx ammonia gas turbine combustor using two-stage combustion

As discussed in Section 4.3, two-stage combustion can be used to achieve low NOx emission from $NH_3$/air non-premixed flames. Kurata et al. [24] recorded NO emissions above 1000 ppm from their combustor, as shown in Fig. 5. Their original combustor, shown in Fig. 34, had air injection holes in the primary and secondary combustion zones. In addition, the circumference of the liner base plate was corrugated, creating gaps between the liner and the sleeve-fitted base plate. These holes upstream of the combustor, i.e., the primary combustion zone, allow the dilution of the flame in the primary zone. In hydrocarbon combustion, such dilution is necessary for thermal NOx control as it reduces the flame temperature. However, in ammonia combustion, the injection of dilution air into the primary zone creates regions of lean combustion which is associated with high NO production. Furthermore, Kurata et al. employed vertical fuel injection parallel to the combustor central axis, $\theta = 0°$. This injection strategy results in low combustion efficiency of ammonia-air flames, and thus leads to a large amount of unburned $NH_3$ being transported from

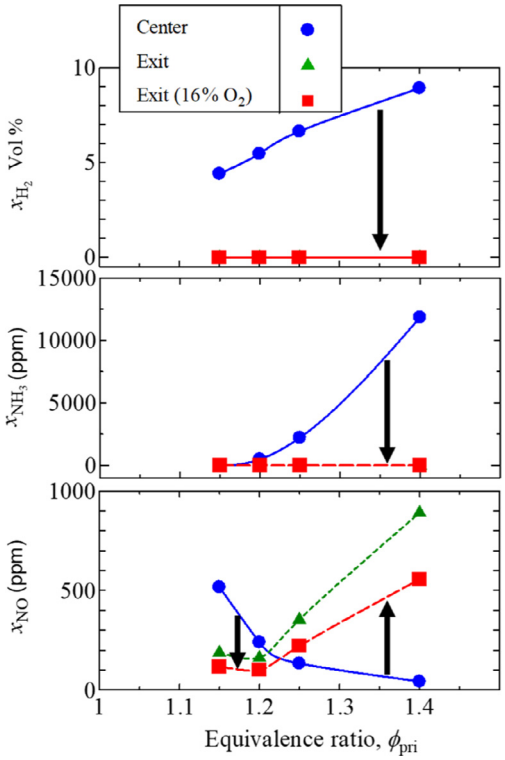


Fig. 33. Effect of secondary air injection on space and time averaged emissions of NO, $NH_3$ and $H_2$ at $P_0 = 0.5$ MPa. Reprinted from [134] with permission from Elsevier.

the primary zone to the secondary zone. This has been reported to promote NOx emission from a two-stage ammonia combustors [137].

More recent data from Kurata and co-workers [138,139] show that significantly lower NOx emission and wider turbine operating power range was achieved by the partial closure of the swirler area, avoidance of any sort of air dilution in the primary combustion zone, and the enhancement of fuel-air mixing by the use of inclined fuel injection. An increase in the fuel injection angle significantly extended the lower operating power limit of the micro gas turbine and NOx emission of 337 ppm (16% $O_2$) was achieved from the micro gas turbine as a result of the modifications made to the combustor.

The present authors conducted laboratory tests on a similarly modified combustor, where all holes in the primary zone, including the gaps at the sleeve fitting, were closed and also the diameter of the secondary holes were reduced from 23 mm to 16 mm. Furthermore, a fuel injector with $\theta = 45°$, with respect to the combustor's central axis, was employed. The combustor was placed inside a high-pressure combustion chamber and air was supplied to the base of the chamber. All the air could pass freely through the combustor. In this air supply

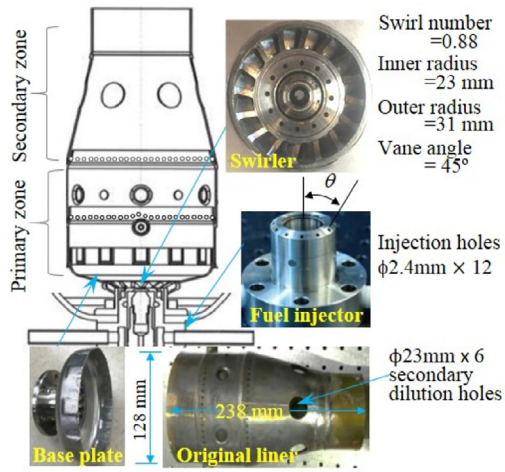


Fig. 34. The described micro gas turbine combustor.

configuration, which is similar to that of a micro gas turbine [24], the overall equivalence ratio, $\phi_{ovr}$, is related to the global equivalent ratio of the primary zone, $\phi_{pri}$, by $\phi_{ovr} = n \cdot \phi_{pri}$. Here, $n$ is the ratio of the air flow rate via the swirler to the total air flow rate. With a secondary hole diameter of 16 mm, the value of $n$ was 0.28. Therefore, $\phi_{ovr}$ was around 0.35 when the primary zone is slightly rich (as in the 3D modelling in Fig. 32). The total air flow rate was 530 LPM at 0.10 MPa and 1060 LPM at 0.20 MPa, hence the swirler inlet velocity was kept constant at 2.78 m/s at all conditions. To initiate combustion, hydrogen was first supplied to the combustor and ignited remotely with a glow plug. Gaseous ammonia was then supplied and the hydrogen supply turned off. The combustor inlet temperature was 298 K. Exhaust gases were sampled from the combustor exit and analyzed using an FTIR (BOB-2000FT, Best Sokki) gas analyzer. Chemical reactions were considered quenched at the point of sampling because the sampling line was maintained at 464 K, which also prevented condensation of $H_2O$ along the line. The combustor outlet temperature (COT) was measured with K-type thermocouples. All these measurements have uncertainties less than or equal to ±20 K.

As shown in Fig. 35, NOx emission varied non-monotonically with $\phi_{pri}$, with an optimum low-NOx $\phi_{pri}$ at slightly rich condition, i.e., $\phi_{sp}$. Figure 35 also shows that NOx emission decreased with pressure. About 90% of the NOx measured from the combustor consisted of NO and the effect of pressure on fuel NO production in ammonia flames has been discussed in Section 3.5. These experimental results agree qualitatively with the results of 3D modelling discussed in Section 4.1 and 4.3.

Although the regulatory limit imposed by the Japanese government for NOx emission from gas

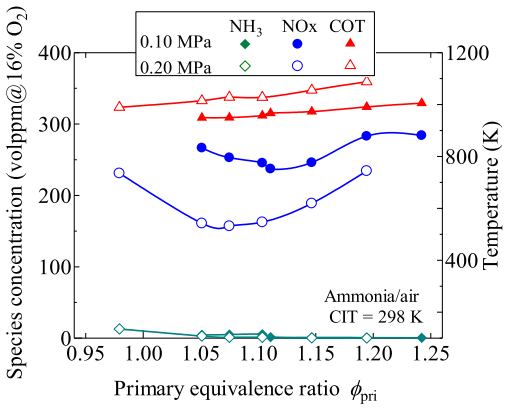


Fig. 35. Emissions recorded from laboratory tests using the described modified ammonia combustor.

turbine is 70 ppm [140], various prefectural governments enforce more stringent limits as low as 10 ppm. Therefore, with the 95% NOx reduction efficiency of ordinary SCR systems, the targeted emission level from ammonia gas turbine combustors is about 200 ppm. The lowest NOx emission obtained from the present study is 157 ppm at a pressure of 0.20 MPa. Using this same combustor while controlling the overall and the primary equivalence ratios independently, Okafor et al. [137] reported NOx emission of 42 ppm with a combustion efficiency of 99.5 % from premixed ammonia-air flames at 0.30 MPa and at $\phi_{sp}$ of 1.10.

## 5. Conclusions

Ammonia synthesis was developed about 100 years ago to increase food production and support the growing world population in the 20th century. In the 21st century, ammonia production using renewable energy can play a significant role in reducing GHG emissions and thus may contribute to mitigating climate change. The advantages of ammonia are not only that it is a hydrogen carrier, but also its availability, amenability to storage and transport, and its utility as a fuel for various energy and industrial applications. The combustion of ammonia, which is the most effective way to use ammonia as an energy source, is a key technology. Challenges such as low flammable characteristics and fuel NOx emission can be overcome by the knowledge of the dynamics and chemistry of combustion. Research and development of ammonia utilization, as well as further development of ammonia synthesis catalysts, will be of increasing interest due to economics and industrial demands. The combustion research community will be able to contribute to economically effective decarbonization of energy systems by developing ammonia combustion technology.

## Acknowledgements

The authors acknowledge Professor Hisashi Nakamura, Professor Gao Wei, Taku Kudo and Tomohiro Nitta for stimulating discussions and assisting with the experiments. We also acknowledge Ph.D. students, Akinori Ichikawa and Sophie Colson, and all of the students in our laboratory for their contributions to the success of the work reported here. Moreover, this material is based on the work supported by the Council for Science, Technology and Innovation (CSTI), the Cross-ministerial Strategic Innovation Promotion Program (SIP) "Energy Carriers" (Funding agency: Japan Science and Technology Agency (JST)). A part of the work was carried out under the Collaborative Research Project of the Institute of Fluid Science, Tohoku University.

## References

[1] United Nations, The Paris Agreement, 2015, available at http://unfccc.int/files/essential_background/convention/application/pdf/english_paris_agreement.pdf.
[2] Ministry of the Environment, Government of Japan, Submission of Japan's Intended Nationally Determined Contribution (INDC) available at https://www.env.go.jp/en/earth/cc/2030indc_mat01.pdf.
[3] United Nations, Kyoto Protocol, available at http://unfccc.int/resource/docs/convkp/kpeng.pdf.
[4] Y. Kojima, H. Miyaoka, T. Ichikawa, Advanced Materials for Clean Energy, Chapt.16, *Ammonia-Based Hydrogen Storage Materials*, CRC Press, 2015.
[5] T. Okanishi, K. Okura, A. Srifa, H. Muroyama, T. Matsui, M. Kishimoto, M. Saito, H. Iwai, H. Yoshida, M. Saito, T. Koide, H. Iwai, S. Suzuki, Y. Takahashi, T. Horiuchi, H. Yamasaki, S. Matsumoto, S. Yumoto, H. Kubo, J. Kawahara, A. Okabe, Y. Kikkawa, T. Isomura, K. Eguchi, *Fuel Cells* 17 (2017) 383–390.
[6] V. Smil, *Popul. Dev. Rev.* 17 (1991) 569–601.
[7] N. Olson, in: The 11th Annual NH3 fuel conference, Des Moines, 2014 available at.
[8] One extra reference NIST Chemistry WebBook, SRD 69, Thermophysical Properties of Fluid Systems, National Institute of Standard and Technology, available at http://webbook.nist.gov/chemistry/fluid/.
[9] http://www.ispt.eu/media/ISPT-P2A-Final-Report.pdf.
[10] C. Philibert, *Insight Series* (2017). available at https://www.iea.org/publications/insights/insightpublications/Renewable_Energy_for_Industry.pdf .
[11] E. Krock, *J. Inst. Petrol.* 31 (213) (1945).
[12] NASA, available at https://www.nasa.gov/centers/armstrong/news/FactSheets/FS-052-DFRC.html.
[13] F.J. Verkamp, M.C. Hardin, J.R. Williams, *Proc. Combust. Inst* 11 (1967) 985–992.
[14] United States of America U.S. Army Engineer Research and Development Laboratories, Solar Division of International Harvester Company,

De- velopment of an Ammonia-Burning Gas Turbine Engine, Final Technical Report, DA-44-009-AMC- 824(T), Fort Belvoir, Solar, 1968, available at http://oai.dtic.mil/oai/oai?verb=getRecord&metadataPrefix=html&identifier=AD0671667.
[15] D.T. Pratt, *Performance of Ammonia-Fired Gas-Turbine Combustors*, Berkley University of California, 1967 Technical Report No.9, DA- 04-200-AMC-791(x)available athttp://www.dtic.mil/dtic/tr/fulltext/u2/657585.pdf.
[16] S. Frigo, R. Gentili, *Int. J. Hydrogen Energy* 38 (2013) 1607–1615.
[17] B. Evans, in: the 10th Annual NH3 fuel conference, Sacramento, 2013 available at https://nh3fuelassociation.org/wp-content/uploads/2013/10/nh3fcx-brian-evans.pdf.
[18] A. Valera-Medina, R. Marsh, J. Runyon, D. Pugh, P. Beasley, T. Hughes, P. Bowen, *Appl. Energy* 185 (2017) 1362–1371.
[19] H. Xiao, A. Valera-Medina, P.J. Bowen, *Energy* 140 (2017) 125–135.
[20] A. Valera-Medina, D.G. Pugh, P. Marsh, G. Bulat, P. Bowen, *Int. J. Hydrogen Energy* 42 (2017) 24495–24503.
[21] D. Pugh, P. Bowen, A. Valera-Medina, A. Giles, J. Runyon, R. Marsh, *Proc. Combust. Inst.* 37 (2018) Article in Press.
[22] Japan Science and Technology Agency, available at http://www.jst.go.jp/sip/pdf/SIP_energycarriers2016_en.pdf.
[23] National Institute of Advanced Industrial Science and Technology, available at http://www.aist.go.jp/aist_j/press_release/pr2015/pr20150917/pr20150917.html.
[24] O. Kurata, N. Iki, T. Matsunuma, T. Inoue, T. Tsujimura, H. Furutani, H. Kobayashi, A. Hayakawa, *Proc. Combust. Inst.* 36 (2017) 3351–3359.
[25] Central Research Institute of Electric Power Industry, available at http://criepi.denken.or.jp/press/pressrelease/2017/01_10press.pdf , (in Japanese).
[26] Japan Science and Technology Agency available at http://www.jst.go.jp/pr/announce/20161031-2/ , (in Japanese).
[27] A. Hayakawa, T. Goto, R. Mimoto, T. Kudo, H. Kobayashi, *Mech. Eng. J.* 2 (2015) 14–00402.
[28] R.W.B. Pearse, A.G. Gaydon, *The Identification of Molecular Spectra*, Fourth Ed., John Wiley & Sons, Inc, 1976.
[29] A. Hayakawa, T. Goto, R. Mimoto, Y. Arakawa, T. Kudo, H. Kobayashi, *Fuel* 159 (2015) 98–106.
[30] K. Takizawa, A. Takahashi, K. Tokuhashi, S. Kondo, A. Sekiya, *J. Hazard Mater.* 155 (2008) 144–152.
[31] U.J. Pfahl, M.C. Ross, J.E. Shepherd, K.O. Pasamehmetoglu, C. Unal, *Combust. Flame* 123 (2000) 140–158.
[32] F.Z. Zakaznov, L.A. Kursheva, Z.I. Felina, *Combust. Explos. Shock Waves* 14 (1978) 710–713.
[33] P.D. Ronney, *Combust. Sci. Technol.* 58 (1988) 123–141.
[34] C.K. Law, Combustion Physics, Cambridge University Press, 2006, p. 347.
[35] E. Hu, Z. Huang, J. He, H. Miao, *Int. J. Hydrogen Energy* 34 (2009) 8741–8755.
[36] E. Varea, V. Modica, A. Vandel, B. Renou, *Combust. Flame* 159 (2012) 577–590.
[37] O. Mathieu, E.L. Petersen, *Combust. Flame* 162 (2015) 554–570.
[38] G.P. Smith, D.M. Golden, M. Frenklach, N.W. Moriarty, B. Eiteneer, M. Goldenberg, et al., GRI Mech 3.0. Gas Research Institute, available at http://www.me.berkeley.edu/gri_mech/.
[39] S. Colson, A. Hayakawa, T. Kudo, H. Kobayashi, *J. Therm. Sci. Technol.* 11 (2016) JTST0048-JTST0048.
[40] K. Takita, H. Yamazaki, T. Uchida, G. Masuya, *Combust. Sci. Technol.* 178 (2006) 1649–1668.
[41] Z. Tian, L. Zhang, Y. Li, T. Yuan, F. Qi, *Proc. Combust. Inst.* 32 (2009) 311–318.
[42] A. Ichikawa, A. Hayakawa, Y. Kitagawa, K.D.KunkumaAmila Somarathne, T. Kudo, H. Kobayashi, *Int. J. Hydrogen Energy* 40 (2015) 9570–9578.
[43] J.H. Lee, J.H. Kim, J.H. Park, O.C. Kwon, *Int. J. Hydrogen Energy* 35 (2010) 1054–1064.
[44] J. Li, H. Huang, N. Kobayashi, Z. He, Y. Nagai, *Int. J. Energy Res.* 38 (2014) 1214–1223.
[45] P. Kumar, T.R. Meyer, *Fuel* 108 (2013) 166–176.
[46] C.S. Mørch, A. Bjerre, M.P. Gøttrup, S.C. Sorenson, J. Schramm, *Fuel* 90 (2011) 854–864.
[47] M. Comotti, S. Frigo, *Int. J. Hydrogen Energy* 40 (2015) 10673–10686.
[48] P.F. Henshaw, T. D'andrea, K.R.C. Mann, D.S.-K. Ting, *Combust. Sci. Technol.* 177 (2005) 2151–2170.
[49] E.C. Okafor, Y. Naito, S. Colson, A. Ichikawa, T. Kudo, A. Hayakawa, H. Kobayashi, *Combust. Flame* 187 (2018) 185–198.
[50] U. Zietz, G. Baumgärtel, *Combust. Flame* 13 (1969) 329–330.
[51] H. Bockhorn, F. Fetting, J.C. Mende, *Combust. Flame* 18 (1972) 471–473.
[52] J. Jójka, R. Ślefarski, *Fuel* 217 (2018) 98–105.
[53] A. Boretti, *Int. J. Hydrogen Energy* 42 (2017) 7071–7076.
[54] K.L. Tay, W. Yang, S.K. Chou, D. Zhou, J. Li, W. Yu, F. Zhao, B. Mohan, *Energy Procedia* 105 (2017) 4621–4626.
[55] H. Takeishi, J. Hayashi, S. Kono, W. Arita, K. Iino, F. Akamatsu, *Trans. JSME* 181 (2015) 14–00423 (in Japanese).
[56] J. Li, H. Huang, N. Kobayashi, Z. He, Y. Osaka, T. Zeng, *Energy* 93 (2015) 2053–2068.
[57] D.G.R. Andrews, P. Gray, *Combust. Flame* 8 (1964) 113–126.
[58] J.W. Armitage, P. Gray, *Combust. Flame* 9 (1965) 173–184.
[59] D.I. Maclean, H.G. Wagner, *Proc. Combust. Inst.* 11 (1967) 871–878.
[60] J. Bian, J. Vandooren, P.J. van Tiggelen, *Proc. Combust. Inst.* 21 (1986) 953–963.
[61] R.P. Lindstedt, M.A. Selim, *Combust. Sci. Technol.* 99 (1994) 253–276.
[62] R.E. Setchell, J.A. Miller, *Combust. Flame* 33 (1978) 23–32.
[63] R. Murai, R. Omori, R. Kano, Y. Tada, H. Higashino, N. Nakatsuka, J. Hayashi, F. Akamatsu, K. Iino, Y. Yamamoto, *Energy Procedia* 120 (2017) 325–332.
[64] E. Rohde, K.R. Löblich, F. Fetting, *Combust. Flame* 13 (1969) 327–329.
[65] N. Peters, *Turbulent Combustion*, Cambridge University Press, 2000.

[66] T.M. Wabel, A.W. Skiba, J.E. Temme, J.F. Driscoll, *Proc. Combust. Inst.* 36 (2017) 1809–1816.
[67] R.K. Lyon, US Patent 3900554, (1975).
[68] R.K. Lyon, *Int. J. Chem. Kinet.* 8 (1976) 315–318.
[69] B.S. Haynes, *Combust Flame* 28 (1977) 81–91.
[70] M.A. Cremer, C.J. Montgomery, D.H. Wang, M.P. Heap, J. Chen, *Proc. Combust. Inst.* 28 (2000) 2427–2434.
[71] N. Cohen, *Int. J. Chem. Kinet.* 19 (1987) 319–362.
[72] J.A. Miller, C.T. Bowman, *Prog. Energy Combust. Sci.* 15 (1989) 287–338.
[73] A.M. Dean AM, J.W. Bozzelli, Combustion chemistry of nitrogen, in: WC Gardiner (Ed.), *Gas Phase Combustion Chemistry*, Springer, New York, 2000 Chapt. 2.
[74] P. Glarborg, J.A. Miller, B. Ruscic, S.J. Klippenstein, *Prog. Energy Combust. Sci* 67 (2018) 31–68.
[75] J.A. Miller, M.C. Branch, R.J. Kee, *Combust. Flame* 43 (1981) 81–98.
[76] J.A. Miller, M.D. Smooke, R.M. Green, R.J. Kee, *Combust. Sci. Technol.* 34 (1983) 149–176.
[77] R.M. Green, J.A. Miller, *J. Quant. Spectrosc. Radiat. Transf.* 26 (1981) 313–327.
[78] C.P. Fenimore, G.W. Jones, *J. Phys. Chem.* 65 (1961) 298–303.
[79] R.C. Murray, A.R. Hall, *Trans. Faraday Soc.* 47 (1951) 743–751.
[80] Ø. Skreiberg, P. Kilpinen, P. Glarborg, *Combust. Flame* 136 (2004) 501–518.
[81] T. Mendiara, P. Glarborg, *Combust. Flame* 156 (2009) 1937–1949.
[82] J. Bian, J. Vandooren, P.J. Van Tiggelen, *Proc. Combust. Inst.* 23 (1990) 379–386.
[83] R.P. Lindstedt, M.A. Selim, *Combust. Sci. Technol.* 99 (1994) 277–298.
[84] J. Vandooren, J. Bian, P.J. Van Tiggelen, *Combust. Flame* 98 (1994) 402–410.
[85] C. Duynslaegher, H. Jeanmart, J. Vandooren, *Proc. Combust. Inst.* 32 (2009) 1277–1284.
[86] A.M. Dean, M. -S Chou, D. Stern, *Int. J. Chem. Kinet.* 16 (1984) 633–653.
[87] A.A. Konnov, *Combust. Flame* 134 (2003) 421–424.
[88] M. Skottene, K.E. Rian, *Int. J. Hydrogen Energy* 32 (2007) 3572–3585.
[89] M.S. Day, J.B. Bell, X. Gao, P. Glarborg, *Proc. Combust. Inst.* 33 (2011) 1591–1599.
[90] D.D. Thomsen, N.M. Laurendeau, *Combust. Flame* 124 (2001) 350–369.
[91] J.B. Bell, M.S. Day, J.F. Grcar, W.G. Bessler, C. Schulz, P. Glarborg, A.D. Jensen, *Proc. Combust. Inst.* 29 (2002) 2195–2202.
[92] H. Guo, G.J. Smallwood, F. Liu, Y. Ju, Ö.L. Gülder, *Proc. Combust. Inst.* 30 (2005) 303–310.
[93] A.A. Konnov, J. De Ruyck, *Combust. Flame* 125 (2001) 1258–1264.
[94] A.A. Konnov, I.V. Dyakov, J. de Ruyck, *Proc. Combust. Inst.* 29 (2002) 2171–2177.
[95] S.J. Klippenstein, L.B. Harding, P. Glarborg, J.A. Miller, *Combust. Flame* 158 (2011) 774–789.
[96] A.A. Konnov, J. De Ruyck, *Combust. Sci. Technol.* 152 (2000) 23–37.
[97] F. Davidson, K. Kohse-Hoinghaus, A.Y. Chang, R.K. Hanson, *Int. J. Chem. Kinet.* 22 (1990) 513–535.
[98] A.A. Konnov, J. De Ruyck, *Combust. Sci. Technol.* 168 (2001) 1–46.
[99] A.A. Konnov, J. De Ruyck, *Combust. Flame* 124 (2001) 106–126.
[100] A.A. Konnov, G. Colson, J. De Ruyck, *Fuel* 80 (2001) 49–65.
[101] A.A. Konnov, *Combust. Flame* 156 (2009) 2093–2105.
[102] G. Shmakov, O.P. Korobeinichev, I.V. Rybitskaya, A.A. Chernov, D.A. Knyazkov, T.A. Bolshova, A.A. Konnov, *Combust. Flame* 157 (2010) 556–565.
[103] C. Duynslaegher, F. Contino, J. Vandooren, H. Jeanmart, *Combust. Flame* 159 (2012) 2799–2805.
[104] H. Nakamura, S. Hasegawa, *Proc. Combust. Inst.* 36 (2017) 4217–4226.
[105] H. Nakamura, S. Hasegawa, T. Tezuka, *Combust. Flame* 185 (2017) 16–27.
[106] P. Dagaut, P. Glarborg, M.U. Alzueta, *Prog. Energy Combust. Sci.* 34 (2008) 1–46.
[107] J.A. Miller, P. Glarborg, *Int. J. Chem. Kinet.* 31 (1999) 757–765.
[108] B. Atakan, A. Jacobs, M. Wahl, R. Weller, J. Wolfrum, *Chem. Phys. Lett.* 155 (1989) 609.
[109] F. Kasuya, P. Glarborg, J.E. Johnsson, K.I.M. Dam-johansen, *Chem. Eng. Sci.* 50 (1995) 1455–1466.
[110] L.A. Curtiss, D.L. Drapcho, J.A. Pople, *Chem. Phys. Lett.* 103 (1984) 437–442.
[111] J.A. Harrison, R.G.A.R. Maclagan, A.R. Whyte, *J. Phys. Chem.* 91 (1987) 6683–6686.
[112] S.F. Selgren, P.W. McLoughlin, G.I. Gellene, *J. Chem. Phys.* 90 (1989) 1624–1629.
[113] S.P. Walch, R.J. Duchovic, C.M.M. Rohlfing, *J. Chem. Phys.* 90 (1989) 3230–3240.
[114] H. Koizumi, G.C. Schatz, S.P. Walch, *J. Chem. Phys.* 95 (1991) 4130–4135.
[115] J.W. Stephens, C.L. Morter, S.K. Farhat, G.P. Glass, R.F. Curl, *J. Phys. Chem.* 97 (1993) 8944–8951.
[116] P. Glarborg, K. Dam-Johansen, J.A. Miller, R.J. Kee, M.E. Coltrin, *Int. J. Chem. Kinet.* 26 (1994) 421–436.
[117] R.P. Lindstedt, F.C. Lockwood, M.A. Selim, *Combust. Sci. Technol.* 108 (1995) 231–254.
[118] J. Park, M.C. Lin, *J. Phys. Chem. A* 101 (1997) 5–13.
[119] P. Glarborg, P. Kristensen, K. Dam-Johansen, J.A. Miller, *J. Phys. Chem. A* 101 (1997) 3741–3745.
[120] J.A. Miller, S.J. Klippenstein, *J. Phys. Chem. A* 104 (2000) 2061–2069.
[121] J.A. Silver, E.C. Kolb, *J. Phys. Chem.* 86 (1982) 3240–3246.
[122] P. Andersen, A. Jacobs, C. Kleinermanns, J. Wolfrum, *Proc. Combust. Inst.* 19 (1982) 11–22.
[123] J.L. Hall, D. Zeitz, J.W. Stephens, J.V.V. Kaspar, G.P. Glass, R.F. Curl, F.K. Tittel, *J. Phys. Chem.* 90 (1986) 2051–2505.
[124] J.A. Silver, C.E. Kolb, *J. Phys. Chem.* 91 (1987) 3713–3714.
[125] Y. Song, H. Hashemi, J.M. Christensen, C. Zou, P. Marshall, P. Glarborg, *Fuel* 181 (2016) 358–365.
[126] H. Xiao, A. Valera-Medina, R. Marsh, P.J. Bowen, *Fuel* 196 (2017) 344–351.
[127] H. Xiao, A. Valera-Medina, *J. Eng. Gas Turbines Power* 139 (2017) 81504.
[128] M.A. Mueller, R.A. Yetter, F.L. Dryer, *Int. J. Chem. Kinet.* 32 (2000) 317–339.

[129] K.J. Hughes, A.S. Tomlin, E. Hampartsoumian, W. Nimmo, I.G. Zsely, M. Ujvari, T. Turanyi, A.R. Clague, M.J. Pilling, *Combust. Flame* 124 (2001) 573–589.
[130] P. Dagaut, A. Nicolle, *Proc. Combust. Inst.* 30 (2005) 1211–1218.
[131] R. Mével, S. Javoy, F. Lafosse, N. Chaumeix, G. Dupre, C.E. Paillard, *Proc. Combust. Inst.* 32 (2009) 359–366.
[132] J. Otomo, M. Koshi, T. Mitsumori, H. Iwasaki, K. Yamada, *Int. J. Hydrogen Energy* 43 (2018) 3004–3014.
[133] K.D.K.A. Somarathne, A. Hayakawa, H. Kobayashi, *J. Fluid Sci. Tech.* 11 (2016) JFST0026.
[134] K.D.K.A. Somarathne, S. Hatakeyama, A. Hayakawa, H. Kobayashi, *Int. J. Hydrogen Energy* 42 (2017) 27388–27399.
[135] A. Hayakawa, Y. Arakawa, R. Mimoto, K.D.K.A. Somarathne, T. Kudo, H. Kobayashi, *Int. J. Hydrogen Energy* 42 (2017) 14010–14018.
[136] K.D.K.A. Somarathne, S. Colson, A. Hayakawa, H. Kobayashi, *Combust. Theory Model.* 22 (2018) 973–997.
[137] E.C. Okafor, K.D.K.A Somarathne, A. Hayakawa, T. Kudo, O. Kurata, N. Iki, H. Kobayashi, *Proc. Combust. Inst.* 37 (2018) in press.
[138] N. Iki, O. Kurata, T. Inoue, T. Matsunuma, T. Tsujimuira, H. Furutani, H. Kobayashi, A. Hayakawa, E.C. Okafor, in: ASME Turbo Expo 2018: Turbomachinery Technical Conference and Exposition, The American Society of Mechanical Engineers, 2018 paper #: GT 2018-75993.
[139] O. Kurata, N. Iki, T. Inoue, T. Matsunuma, T. Tsujimura, H. Furutani, M Kawano, K. Arai, E.C. Okafor, A. Hayakawa, H. Kobayashi, *Proc. Combust. Inst.* 37 (2018) in press.
[140] Ministry of Environment, Government of Japan, Regulatory measures against air pollutants emitted from factories and business sites and the outline of regulations- Emission Standards for soot, dust, and NOx (1998) Available at: https://www.env.go.jp/en/air/aq/air/air4_table.html

View publication stats